InkSight: Offline-to-Online Handwriting Conversion by Learning to Read and Write

Anonymous authors
Paper under double-blind review

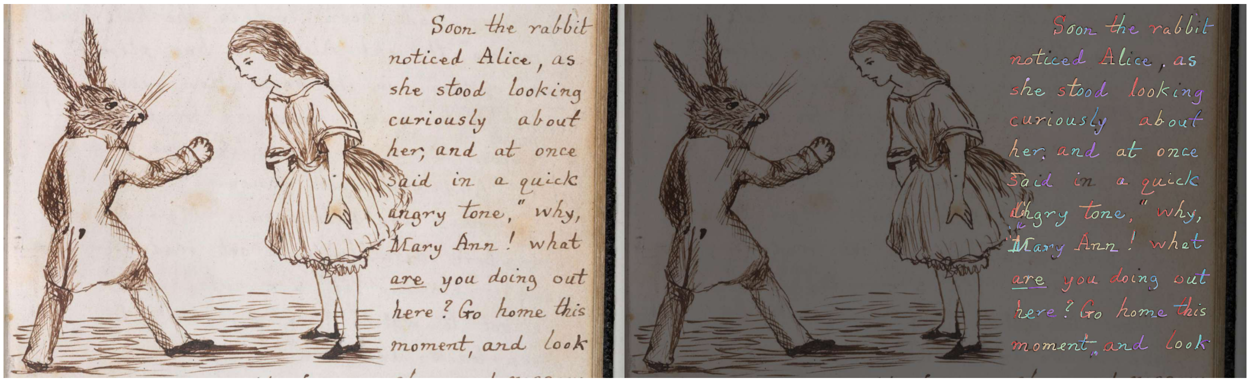

Soon the rabbit
noticed Alice, as
she stood looking
curiously about
her, and at once
said in a quick
angry tone, " why,
Mary Ann! what
are you doing out
here? Go home this
moment, and look

Figure 1: **Results of `InkSight`** [Visualize in gif]. **Left:** A photo of handwritten text (offline handwriting), **Right:** Output digital ink (online handwriting). In every word, character colors transition from red to purple, following the rainbow sequence, ROYGBIV; within each stroke, the shade progresses from darker to lighter. More visualizations in Appendix B.

Abstract

Digital note-taking is gaining popularity, offering a durable, editable, and easily indexable way of storing notes in a vectorized form, known as digital ink. However, a substantial gap remains between this way of note-taking and traditional pen-and-paper note-taking, a practice that is still favored by a vast majority. Our work `InkSight`[1], aims to bridge the gap by empowering physical note-takers to effortlessly convert their work (offline handwriting) to digital ink (online handwriting), a process we refer to as **derendering**. Prior research on the topic has focused on the geometric properties of images, resulting in limited generalization beyond their training domains. Our approach leverages vision-language models to combine *reading* and *writing* priors, allowing training a model in the absence of large amounts of paired samples, which are difficult to obtain. To our knowledge, this is the first work that effectively derenders handwritten text in arbitrary photos with diverse visual characteristics and backgrounds. Furthermore, it generalizes beyond its training domain into simple sketches. Our human evaluation reveals that 87% of the samples produced by our model on the challenging HierText dataset are considered as a valid tracing of the input image and 67% look like a pen trajectory traced by a human.

1 Introduction

Handwritten notes have been a cornerstone of information storage for centuries. Today, with the rise of stylus and digital pen technologies, digital inking is a compelling alternative. This modern approach to storing information offers several advantages: enhanced durability and organization of notes, as well as seamless integration with other types of digital content (images, text, links) or digital assistants. Despite these apparent benefits, many people still prefer traditional handwritten notes over the digital format.

---

[1] The instructions for running the model, model weights (public version: Small-p), inference code, and results are available in the supplementary of our submission.

Our work aims to make physical notes, particularly handwritten text, available in the form of digital ink capturing the stroke-level trajectory details of handwriting. This allows users who prefer conventional ways of note-taking to enjoy the benefits of digital notes without the need to write with a stylus. The topic of converting handwritten text into digital ink has gained significant interest in both academia (Nguyen et al., 2021; Chen et al., 2022b; Mohamed Moussa et al., 2023) and industry (Not, 2023), with the introduction of software solutions that digitize handwriting and hardware solutions that require smart pens and/or special paper (Liv, 2024; Roc, 2024; Neo, 2024). Our approach requires only a picture of the handwritten note, without requiring specialized equipment. It differs from the methods that rely on geometric priors, where gradients, contours, and shapes in an image are utilized to extract writing strokes. Instead, we harness the power of learned *reading* and *writing* priors, where:

- The learned *reading* prior enhances the model's capability to precisely locate and extract textual elements from images. This is achieved either through the model's textual understanding ability or aided with external textual input, e.g. from an OCR engine.
- The integration of the *writing* prior ensures that the resulting vector representation, the digital ink, closely aligns with the typical human approach to writing in terms of physical dynamics and the order of strokes.

To the best of our knowledge, our work is the first to incorporate these priors, resulting in a robust model that is capable of derendering handwriting across diverse scenarios and appearances, including challenging lighting conditions, noticeable occlusions, etc. Our model adopts a simple architecture combining the widely popular and readily available ViT (Dosovitskiy et al., 2021) encoder and an mT5 (Xue et al., 2021) encoder-decoder, fostering reproducibility, reusability, and ease of adoption. To summarize, the major contributions of our work are:

1. We propose the first system to perform **derendering**: transforming arbitrary photos of handwritten text into digital ink. It relies only on the standard architecture components and the training and inference setup that works without expensive data collections and scales to arbitrarily large input images.
2. We show that the inks produced by our system are both semantically and geometrically similar to the input images. We demonstrate that they are similar to real digital ink data, as measured by both automatic and human evaluations.
3. We show that, due to the learned reading and writing priors, our approach is robust well beyond its training data and works on various types of handwriting, simple sketches, and full pages of notes.
4. We release the weights and inference code for the public model Small-p, trained entirely on publicly available datasets, along with a subset of model-generated in universal `inkML` format and human expert digital ink data to support reproducibility and future research on the topic.

2 Related Work

Pen trajectory recovery has been a task of interest to many researchers due to its utility for tasks that can benefit from stroke order / temporal information such as online handwriting recognition (Lallican et al., 2004; Viard-Gaudin et al., 2005; Zhang et al., 2015; Chan, 2020). Another point of interest is the ability to efficiently store, index, and edit handwritten notes within existing online note-taking systems. Classical approaches commonly consist of domain-specific preprocessing (e.g. noise removal, image binarization, skeletonization), local (sub-)stroke level processing (e.g. identification of junction points) and global aggregation (usually as a graph-based optimization problem) (Jager, 1996; Kato & Yasuhara, 2000; Qiao et al., 2006; Chan, 2020; Doermann et al., 2002). These approaches often rely on the quality of the preprocessing and hand-designed heuristics and do not generalize well to other scripts and domains. More recent methods use convolutional (Nguyen et al., 2021; Archibald et al., 2021) and/or recurrent (Bhunia et al., 2018; Chen et al., 2022b) neural networks to translate an image into a sequence of coordinates. Set, sort! (Mohamed Moussa et al., 2023) use two Transformer models to first encode the substrokes of the input and then reorder them, given the encodings. Those methods produce promising results, but focus on the simplified setups of rendered online handwriting and/or single characters.

Line drawing vectorization shares many features with geometric approaches to pen trajectory recovery, but does not include stroke order reconstruction. Recent techniques for this problem involve solving an optimization task of fitting a set of geometric primitives (e.g. Bezier curves) to match the geometric and/or semantic content of the input image (Vinker et al., 2022), sometimes relying on differentiable rendering to maintain the inputs and outputs in the image space (Mo et al., 2021). These approaches focus on converting raster images (perfectly aligned, clean, clear backgrounds) to vector ones. Thus they avoid dealing with the realistic photo artifacts related to lighting, noisy backgrounds or photo-taking angles. These artifacts are however unavoidable in a real-world setting.

Dataset availability is limiting the research in trajectory recovery as there are few datasets of images and their corresponding digital inks. These include IRONOFF (Viard-Gaudin et al., 1999), CASIA (Liu et al., 2011), IBM-UB (Shivram et al., 2013) for handwritten text (images there exhibit limited variability being always black-on-white line writing, usually on the same input device) and Sketchy (Sangkloy et al., 2016) for crowd-sourced sketches of photos from 125 object categories.

Combining language models with new modalities is related to this work since we convert the pen trajectory to a sequence of coordinates on a fixed size canvas and represent the coordinates with *ink tokens* (more details in Section 3.3). Hence, we consider our approach as extending a Visual Language Model (VLM) with a new modality. Recent research in this area has been pointed towards training adapters for merging the pretrained unimodal models (e.g. Alayrac et al. (2022)) or, fully or partially fine-tuning a system with multi-modal tasks (e.g. Chen et al. (2022a)). Works most similar to ours are AudioPaLM (Rubenstein et al., 2023), extending LLM with audio tokens, Painter (Pourreza et al., 2023) using coordinate-based representation of strokes to perform generation and understanding of sketches, and PixelLLM (Xu et al., 2024) using the same representation to localize words in the image caption.

3 Method

While the fundamental concept of derendering appears straightforward – training a model that generates digital ink representations from input images – the practical implementation for arbitrary input images presents two significant challenges:

1. **Limited Supervised Data:** Acquiring paired data with corresponding images and ground truth digital ink for supervised training can be expensive and time-consuming and no datasets with sufficient diversity exist for this task yet.
2. **Scalability to Large Images:** The model must effectively handle potentially arbitrary large input images with varying resolutions and amounts of content.

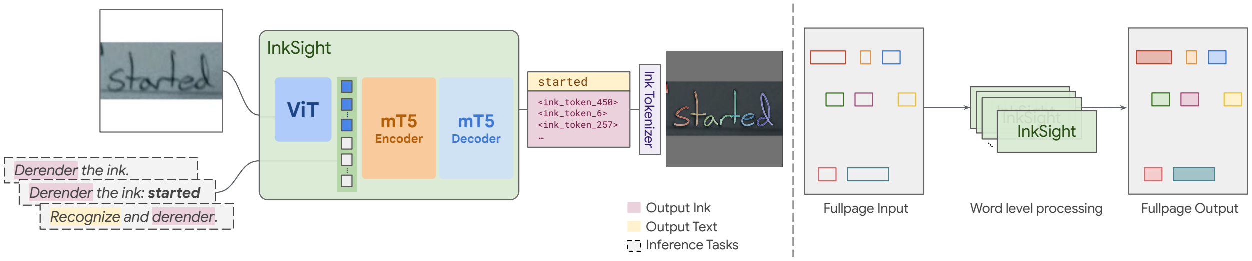

Figure 2: **Left:** Illustration of model inference. Inputs include an image and a prompt specifying the task. Outputs may consist of ink alone or a combination of ink and text, as indicated by matching colors in both the input prompt and the output. Ink tokens are detokenized into digital ink using our proposed ink tokenizer explained in Section 3.3. **Right:** Diagram of the Full Page System. [Illustration in gif]

To address the first problem without expensive data collection, we propose a multi-task training setup that combines recognition and derendering tasks. We show that this setup enables the model to generalize on derendering tasks with various styles of images as input, and injects the model with both semantic understanding and writing priors of handwritten text. We discuss our data and multi-task training setup in Section 3.2, and ablate the design choices in Section 4.6. The exact model structure, which consists of standard publicly available off-the-shelf components, is discussed in Section 3.1. In Section 3.3, we cover the representation of digital ink, the normalization of the data, and the tokenization scheme we employ.

The second problem can be addressed by training a model with very high-resolution input images and very long output sequences, but this is computationally prohibitive. Instead, we break down the derendering of a page of notes into three steps: running OCR to extract word-level bounding boxes, derendering each of the words separately and pasting the derendered words back, as shown in Figure 2. An example of full page inference is shown in Figure 1, more full page results are presented in Appendix M.

3.1 Vision-Language Model for Digital Ink

Our model architecture, inspired by that of PaLI (Chen et al., 2022a; 2023b;a), integrates a Vision Transformer (ViT) encoder (Dosovitskiy et al., 2021) with an mT5 encoder-decoder Transformer model (Xue et al., 2021). We provide the task-specific instructions as text, as described in Section 3.2. We use the same set of tokens for both input and output, which contains the individual character tokens from the original mT5 vocabulary and specific tokens reserved for the ink representation (details in Sec. 3.3). To initialize the model, we use the pre-trained weights of the ViT encoder. The mT5-based encoder-decoder weights are initialized randomly, which is motivated by our customized token dictionary differing from the one used in mT5's original training. In our training, we freeze the weights of the ViT encoder – we justify this choice empirically in Section 4.6.

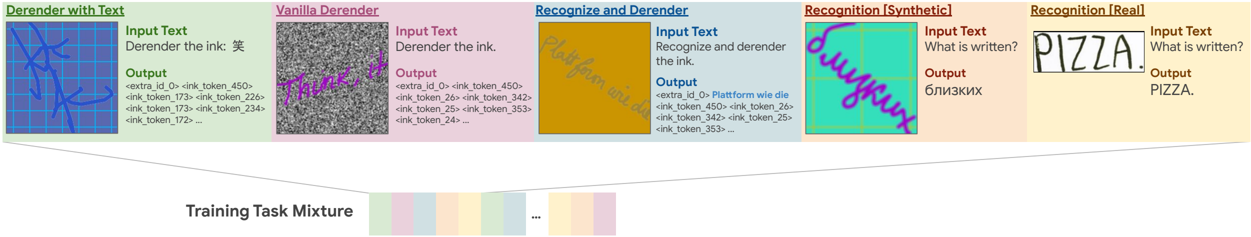
Derender with Text
Input Text
Derender the ink: 笑
Output
<extra_id_0> <ink_token_450> <ink_token_173> <ink_token_226> <ink_token_173> <ink_token_234> <ink_token_172> ...
Vanilla Derender
Think, it
Input Text
Derender the ink.
Output
<extra_id_0> <ink_token_450> <ink_token_26> <ink_token_342> <ink_token_25> <ink_token_353> <ink_token_24> ...
Recognize and Derender
Plattform wie die
Input Text
Recognize and derender the ink.
Output
<extra_id_0> Plattform wie die <ink_token_450> <ink_token_26> <ink_token_342> <ink_token_25> <ink_token_353> ...
Recognition [Synthetic]
близких
Input Text
What is written?
Output
близких
Recognition [Real]
PIZZA.
Input Text
What is written?
Output
PIZZA.
Training Task Mixture
...

Figure 3: **Illustration of multi-task training mixture.** The training mixture comprises five different task types: two derendering tasks (ink output), two recognition tasks (text output), and one mixed task (text-and-ink output). Each type of task utilizes a task-specific input text, enabling the model to distinguish between tasks during both training and inference.

3.2 Training Task Mixture

To circumvent the challenge of not having diverse paired image and ink samples as training data, we propose a multi-task training setup comprising two derendering tasks, two recognition tasks, and one hybrid task (shown in Figure 3 and described in Table 1).

Table 1: Summary of tasks in our proposed multi-task training.

Task	**Description**
Vanilla Derender	The model receives a synthetic ink image with a conditioning task prompt and outputs ink tokens corresponding to the image content.
Derender with Text	The model receives a synthetic ink image and a task conditioning prompt including the target textual content, and outputs ink tokens corresponding to the provided text within the image.
Recognition (Syn/Real)	The model receives an ink image (either synthetic or real) and a task conditioning prompt and outputs the recognized textual content. This task uses both synthetic ink images and real images from OCR datasets.
Recognize and Derender	This task combines recognition and derendering. The model receives a synthetic ink image and a prompt and outputs both the recognized text and the corresponding ink tokens.

We show that this setup helps the model to: (1) generalize to the derendering of real photos; (2) learn useful priors that help deal with occlusions and generate realistic ink; (3) allow using different inference setups that enable, e.g. high-quality text derendering with OCR result (*Derender with Text*) or derendering without textual input for non-textual elements (*Vanilla Derender*). Training tasks are shuffled and assigned equal appearance probability (20%). For best performance during inference, we use *Derender with Text* (this choice is ablated in Section 4.6 where we show that our model performs well without reliance on OCR as well).

Data augmentation. To narrow the domain gap between the synthetic images of rendered inks and the real photos, we augment the data in tasks that take rendered ink as input. This is done by randomizing the ink angle, color, stroke width, and by adding Gaussian noise and cluttered backgrounds. Examples are provided in Figure 3, more details are given in Appendix F, and Section 4.6 highlights the importance of having the data augmentation.

3.3 Data representation

Digital Ink tokenization. Digital ink is usually represented as a sequence of strokes $I = \{s_1, s_2, \cdots, s_n\}$, where each stroke s_i consists of a sequence of m_i (length of the i-th stroke) coordinate-time triplets, represented as $s_i = \{(x_i, y_i, t_i)\}_{i=1}^{m_i}$. To enable sequence models like mT5 to generate ink strokes, we first normalize the ink and then tokenize it into a set of discrete tokens from a pre-defined dictionary. Normalizing the ink includes:

1. **Resampling:** Resample the ink at a fixed frequency (20 ms) to account for potential variations between input devices.
2. **Sequence Reduction:** Apply Ramer-Douglas-Peucker resampling (Visvalingam & Whyatt, 1990) to reduce the sequence length while preserving the overall shape of the strokes.
3. **Normalization:** Shift and scale the ink strokes to position them at the center of a fixed-size canvas. Each point in a stroke is scaled to fit within the range $[0, N]$, where we use $N = 224$ in our implementation.

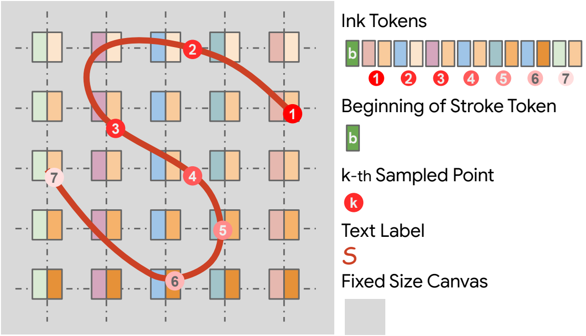

Figure 4: **Ink tokenization for a single-stroke digital ink [Illustration in gif].** The dark red ink depicts the normalized ink stroke, with numbered circles marking sampled points after time resampling. The color gradient of the sampled points indicates the point order. Each point is represented with two tokens encoding its x and y coordinates. The token sequence for this ink begins with `b`, signifying the beginning of the stroke, followed by the tokens for coordinates of sampled points.

As shown in Figure 4, tokenization of the normalized ink involves prepending a ***beginning of stroke*** token followed by the x and y coordinates of each point inside the stroke, rounded to the nearest integer value. This is done for every stroke inside the digital ink. The total dictionary size is $2N + 3$ with separate set of tokens for x and y, including $N + 1$ possible x and y values and a token indicating a start of the stroke. N controls the tradeoff between rounding error and vocabulary size, and we use $N = 224$ in practice.

Image representation. For the derendering tasks of the training mixture, we render digital inks in the center of an $M \times M$ image with stroke width, color, and background color selected via random augmentation (see Appendix F). For the recognition task training and inference with real images, we apply a similar transformation: the input image is scaled, centered, and padded in black to produce an $M \times M$ image. Although we use $M = 224$, by design there are no constraints to have $N = M$.

Expanding text vocabulary with Ink. Our set of tokens contains all individual symbols from the multilingual mT5 tokenizer (Xue et al., 2021) (approx. 20k), with additional $2N + 3$ tokens reserved for the representation of the digital ink, as described above. Removing all multi-symbol tokens allows to reduce the size of the input text embedding and final softmax of the decoder model by $\sim 80\%$, while maintaining the ability to input and output arbitrary text and not affecting the quality of derendering or recognition.

4 Experiments

In this section, we discuss the training datasets and implementation details, and present the qualitative and quantitative results, followed by an ablation study on training tasks and design choices.

4.1 Datasets

We train two different models using two types of datasets: one trained only on publicly available data and one trained on our in-house proprietary data. Below, we detail the public datasets and provide aggregated statistics for the in-house counterparts. Additional details are provided in Appendix C.

OCR training data. As public OCR training data, we use RIMES (Augustin et al., 2006; Grosicki et al., 2009), HierText (Long et al., 2022; 2023), IMGUR5K (Krishnan et al., 2023), ICDAR'15 historical documents (Murdock et al., 2015), and IAM (Marti & Bunke, 1999). We crop out word-level images where possible, acquiring 295 000 samples with text in Latin script. The in-house dataset consists of images of handwritten and printed text (67% and 33% respectively) written on a diverse set of backgrounds, with 95% of the labels in English.

For data sources that contain word-level segmentation, we extract images of individual words based on their bounding boxes. For others, we found it beneficial to heuristically filter the training data to exclude samples that are too short, too long, or of too low resolution to be rendered on a 224 × 224 image. The filtering rules ensure that the aspect ratio satisfies $(0.5 < \text{width} / \text{height} < 4.0)$, and that the image size is at least 25 pixels per side.

Digital ink training data. As public digital ink training data, we use VNOnDB (Nguyen et al., 2018), SCUT-Couch (Li et al., 2008), and DeepWriting (Aksan et al., 2018). For DeepWriting we use the available segmentation information to produce 3 datasets with character-level, word-level, and line-level croppings, and use all 3 for training. For VNOnDB we extract individual words to be used as training data. The public dataset size totals ~2.7M samples.The in-house multilingual dataset primarily comprises short snippets of text in Mandarin (37%) and Japanese (23%), while the remaining languages each contribute less than 5%.

Evaluation Data. Since there are no available diverse datasets of paired inks and images (as discussed in Section 2), we perform the evaluation on OCR data and additionally do a small data collection to obtain paired samples. To automatically assess our models, we evaluate the quality of derendering on the test splits of 3 OCR datasets: IAM (`testset_f`, ~17.6k samples), IMGUR5K (~23.7k samples), and HierText. For HierText, which was not originally designed around handwritten samples, we apply the same filtering as to the OCR training data, and additionally only consider words marked as handwritten (~1.3k samples).

Additionally, we have performed a small annotation campaign, asking people to trace ~200 samples from the HierText test set. We use these as the "golden" set to find the reference point in the automated evaluation and as a control group when doing the human evaluation.

4.2 Models

We train 3 variants of our model: **Small-p** (~340M parameters, **-p** stands for **p**ublic setup) trained on publically available datasets with a ViT B/16 encoder pretrained on ImageNet-21k (Deng et al., 2009) paired with an mT5-base encoder-decoder; **Small-i** (**-i** stands for **i**n-house setup), built with the same architecture as Small-p, but using a JFT-300M (Sun et al., 2017) pretrained ViT B/16 checkpoint; **Large-i** (~1B parameters) with a ViT L/16 encoder pretrained on JFT-300M, paired with an mT5-large encoder-decoder. All models employ a context length of 1024 for the output, and 128 for the input. Implementation details are provided in Appendix G, and a model card for Small-p in Appendix L.

4.3 Baseline Method

Despite pen trajectory recovery being a popular research direction in the last decades, available comparisons are limited due to the scarcity of open-sourced code, training data, and pre-trained model weights. Appendix D offers a detailed analysis of recent work and their reproducibility. We choose the General Virtual Sketching (GVS) Framework (Mo et al., 2021) as our baseline. Originally trained for sketch and photo vectorization, GVS offers a valuable reference point despite the domain discrepancy between sketches and handwritten notes. We found that providing the GVS line drawing vectorization model with binarized inputs yields best performance, we compare all 3 available models on original and binarized inputs in Appendix H.

4.4 Qualitative Evaluation

We compare the performance of our models and GVS on 3 public evaluation datasets (mentioned in Section 4.1) in Figures 5 and 6. Our models mostly produce results that accurately reflect the text content, disregarding semantically irrelevant background. They can also handle occlusions, highlighting the benefit of the learned *reading* prior, in contrast to GVS, which produces multiple duplicate strokes, and does not distinguish between background and foreground (which is reasonable, given it was trained for sketch vectorization). **Large-i** is able to retain more details and accommodate more diverse image styles.

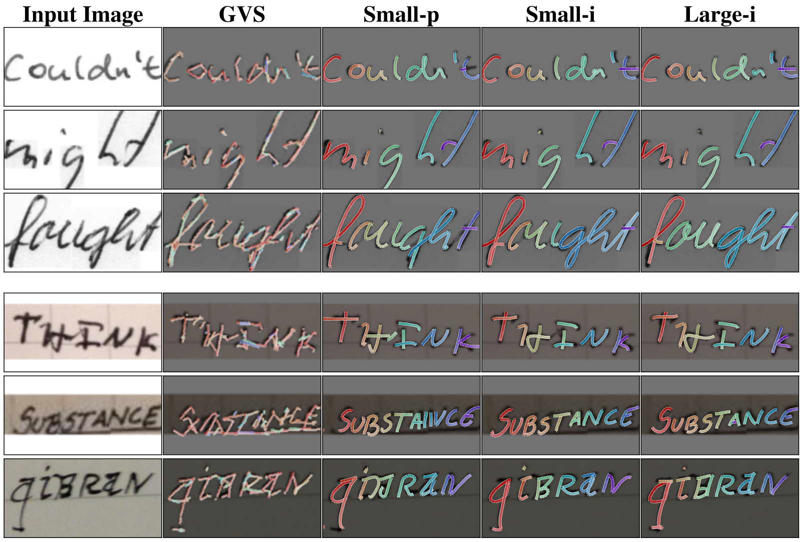

Figure 5: Comparison between performance of GVS, **Small-i**, **Small-p**, and **Large-i** on IAM (top) and IMGUR5K (bottom), more visualizations in Appendix M.1.

Generalization to Sketches. We additionally study the performance of our models on out-of-domain samples, such as simple sketches. For this, we use the *Vanilla Derender* inference mode to obtain the inks. In Figure 7, we observe that our models partly generalize to sketches, but the performance varies significantly depending on the sample and has noticeable artifacts such as missing details or over-focusing on a segment and over-tracing it. They, however, demonstrate robustness to complicated backgrounds (e.g. the lighting of the coffee sample).

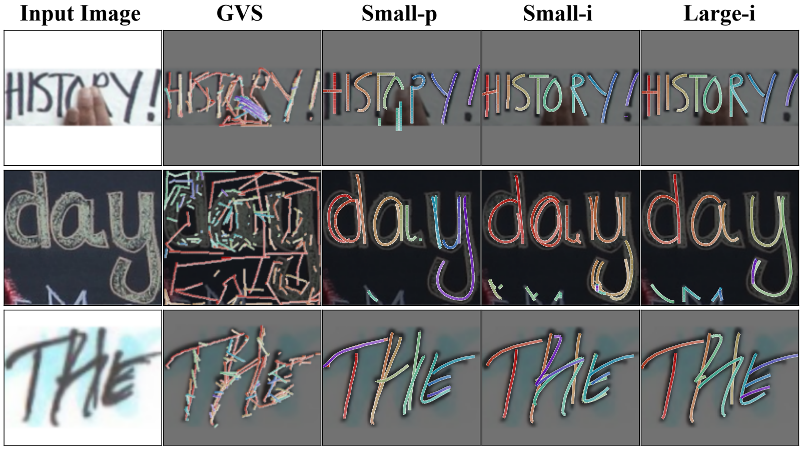

Figure 6: Comparison between performance of GVS, **Small-i**, **Small-p**, and **Large-i** on HierText, which includes data with varying styles and occlusions.

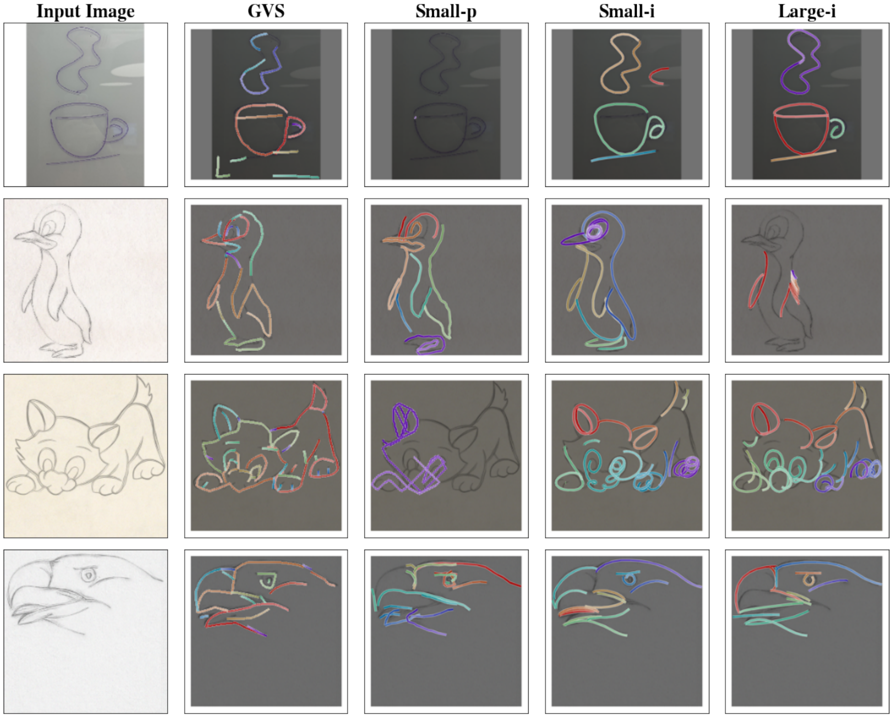

Figure 7: Sketch derendering for **Small-p**, **Small-i**, **Large-i** and GVS. Our models are mostly able to derender simple sketches, however with significant artifacts: missing strokes (e.g the cat), creating cycles (e.g the eye of the penguin for Small-i, the paws of the cat for Large-i) or unnatural strokes (e.g. for Small-p).

4.5 Quantitative Comparison

To support the claims about the performance of our model, we conduct both human evaluation and automated evaluation that compare the similarity of our model output to the original image and to real digital inks. To the best of our knowledge, there are no established metrics and benchmarks for this problem yet.

4.5.1 Human evaluation

We performed a human evaluation of the quality of the derendered inks produced by the three variants of our model. We used the "golden" human traced data on the HierText dataset as the control group and the output of our model on these samples as the experiment group. Evaluators were shown the original image alongside a rendered digital ink, which was either model-generated or human-traced (unknown to the evaluators). They were asked to answer two questions:

1. Is the digital ink output a reasonable tracing of the input image? (Answers: Yes, it's a good tracing; It's an okay tracing, but has some small errors; It's a bad tracing, has some major artifacts);
2. Could this digital ink output have been produced by a human? (Answers: Yes; No).

We provide a more detailed description of the task and the instructions in Appendix K. The evaluation included 16 individuals familiar with digital ink, but not involved in this research. Each sample was evaluated by 3 raters and aggregated with majority voting (with inter-rater reliability κ : (1) 0.46, (2) 0.44 for the respective questions).

We demonstrate the results of our evaluation campaign in Figure 8. We observe better performance (good or okay rating, more realistic samples) when both the data and model size are scaled up. The most common imprecisions that lead to choosing "okay tracing" over "good tracing" include: a small number of extra strokes (e. g. derendering irrelevant elements present in the image), missing details (e.g. punctuation, a dot over i, j), and unnecessary double strokes (see Appendix K for examples).

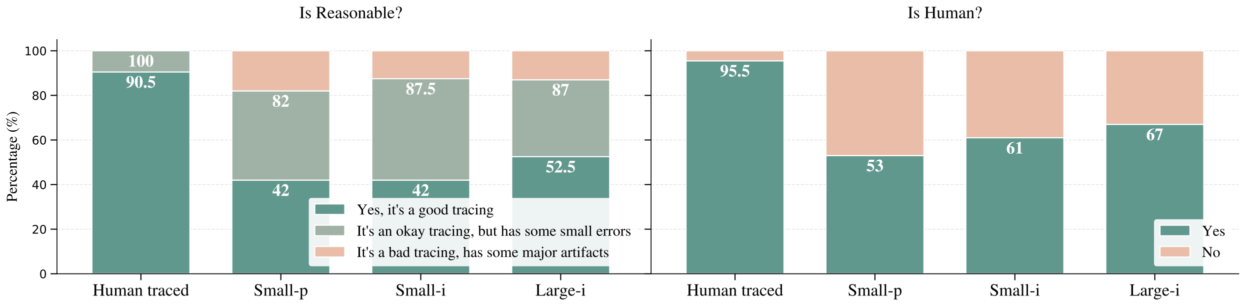

Figure 8: **Human evaluation results for Small-p, Small-i and Large-i** on 200 "golden" samples of HierText dataset.

4.5.2 Automated Evaluation

Automated metrics (described below) are presented in Table 2. Most importantly, the ordering using the automated metrics of our models matches the results of the human evaluation.

Similarity to the input image. To capture how similar the output of our model is to the input image semantically and geometrically, we compute the Character Level F1 score by following the protocol of the Robust Reading Challenge (Rob, 2023). This measure captures both geometry and semantics by counting the character bounding boxes found by an OCR model (in the original input image and in the output of the model rendered as an image) that both overlap significantly and match content-wise. To obtain those character bounding boxes, we use the publicly available API (Clo, 2024). We see that our models perform similarly to GVS on simpler black-on-white IAM dataset, but outperforms it on HierText which has more diverse background. We also note that the OCR engine used is not perfect, and due to errors in the OCR model and its sensitivity to line width, the value of this metric is 0.64 for the "golden" human traced data on

Table 2: Automated metrics comparison between three variants of our model, GVS, and the “golden” human traced data. We compare both Character Level F1 score of the rendered characters and Accuracy of recognizing the generated digital ink with state-of-the-art recognizers.

Model	IAM		IMGUR5K		HierText	
	F1	Acc.	F1	Acc.	F1	Acc.
Small-p	0.65	0.60	0.47	0.33	0.53	0.37
Small-i	0.65	0.59	0.51	0.33	0.61	0.44
Large-i	0.66	0.58	0.51	0.32	0.61	0.46
GVS	0.69	0.02	0.51	0.01	0.55	0.01
Human*	–	–	–	–	0.64	0.74

* Computed on the human-traced subset of HierText data.

HierText. Therefore, it can only be used to meaningfully distinguish models as long as their F1 score is fairly low.

Similarity to the real digital ink data. To assess the semantic consistency and geometric properties of our generated digital inks, we compute recognition Exact Match Accuracy with the state-of-the-art online handwriting recognizer trained on real digital ink data[2]. As shown in Table 2, our models demonstrate superior accuracy compared to GVS (on which the online handwriting recognizer is failing completely due to unnatural stroke number, length and order). We also observed that while the three model variants perform similarly on the IAM and IMGUR5K datasets, the **Large** variant outperforms **Small** variants on the HierText dataset which has greater diversity, which aligns with our human evaluation.

To further validate the similarity between real and derendered digital inks, we train an online handwriting recognizer on inks derendered from the IAM training set. Testing on the `testset_f` of IAMOnDB (Liwicki & Bunke, 2005) and compare with the performance of model trained on IAMOnDB train set, in terms of Character Error Rate metric (CER). As shown in Figure 9, the model trained only on derendered inks achieves slightly worse CER performance compared to the model trained on real data. Furthermore, the combination of derendered IAM inks and real IAMOnDB inks allows to acquire a more diverse training set, resulting in significantly lower CER. This results holds for **Small-p** and **Large-i** as well (see Appendix I). While our CER trails state-of-the-art CER due to limited training data, our work demonstrates that offline handwriting datasets can effectively augment online recognizer training. The details of the online handwriting recognizer we train are given in Appendix I.

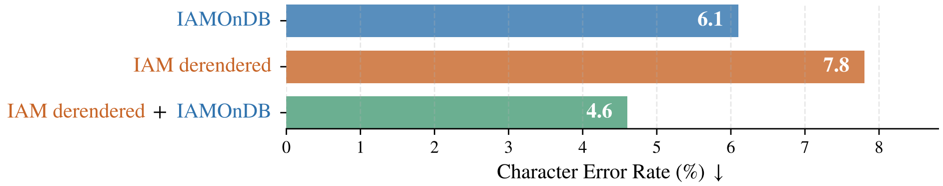

Figure 9: Online handwriting recognition results on IAMOnDB test set for Small-i trained on real digital inks (IAMOnDB train set), derendered digital inks (from IAM train set) and their combination.

4.6 Ablation Studies

This section examines the performance variation across inference tasks and ablates the impact of augmentation, data mixture, and training strategies on the **Small-i** model’s performance. Conclusions and numerical results of the ablation study are presented in Table 3 and summarized below. For more details, see Appendix E.

---

[2] Reference removed for anonymity

Table 3: Ablation studies on **Small-i**. The first row shows the best performance setup (with inference mode *Derender with Text*). Subsequent rows display results for the *Vanilla Derender* and *Recognize and Derender* (R + D) tasks (Figure 3), followed by the impact of various design choices on performance.

Setup	IAM		IMGUR5K		HierText	
	F1	Acc.	F1	Acc.	F1	Acc.
Small-i†	$0.66_{\pm 0.07}$	$0.59_{\pm 0.01}$	$0.51_{\pm 0.09}$	$0.33_{\pm 0.02}$	$0.61_{\pm 0.07}$	$0.45_{\pm 0.01}$
Vanilla	0.61↓	0.53↓	0.44↓	0.28↓	0.53↓	0.35↓
R+D	0.62↓	0.57↓	0.46↓	0.32	0.57↓	0.42↓
Remove						
data aug*	0.42↓	0.33↓	0.21↓	0.09↓	0.23↓	0.13↓
syn rec	0.58↓	0.50↓	0.50↓	0.25↓	0.56↓	0.38↓
real rec	0.64↓	0.50↓	0.55↑	0.19↓	0.59↓	0.36↓
all rec	0.65	0.51↓	0.55↑	0.22↓	0.61	0.38↓
frozen ViT†	$0.65_{\pm 0.13}$	$0.53_{\pm 0.06}$↓	$0.43_{\pm 0.24}$↓	$0.31_{\pm 0.06}$	$0.59_{\pm 0.15}$	$0.41_{\pm 0.05}$↓

* Digital ink rendered as fixed-width white strokes on black background.

† The results are aggregated from three random initializations, all other results are acquired with the best performing initializations with the same three seeds.

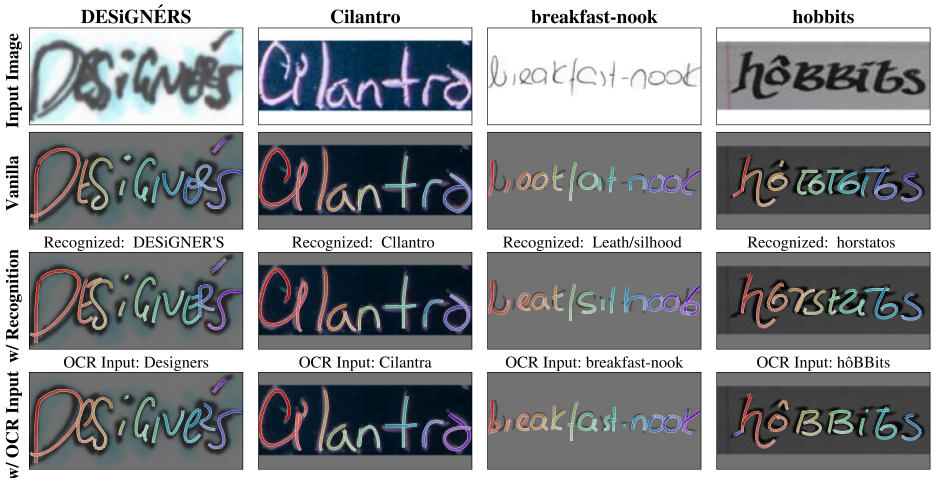

Figure 10: Varied digital ink outputs from **Small-i** inference tasks on samples with ambiguous transcription. Column titles correspond to the ground truth labels. Image titles correspond to either the recognition result from our model or an OCR system.

Inference task matters in difficult cases (Rows 2-3). We compare the performance between three types of inference tasks, we find *Derender with Text* is slightly better than *Recognize and Derender* (R+D), which itself outperforms *Vanilla Derender* on all three datasets, we attribute this difference to the fact that it generates more semantically consistent. Figure 10 shows a collection of derendered inks from **Small-i** where each input image has ambiguous or difficult-to-read characters. We take the first column, `DESiGNÉRS`, as an example: Inference with *Vanilla Derender* captures the overall geometry of the input image but often lacks textual understanding (e.g., the letter `E` and `ÉR` are drawn as rough strokes rather than following the precise structure of the characters). *Derender with Text* produces results consistent with the text input to the model provided by OCR (upper case `E` and `ER`), while *Recognize and Derender* aligns with the model's own recognition, resulting in lowercase `e` and `er`). More examples in Appendix E.2.

The necessity of data augmentation (Row 5). Removing the data augmentation leads to significantly worse performance across all metrics on all datasets. While data augmentation (as shown in Figure 3) does not visually align rendered inks with real ink photos, it diversifies the rendered ink distribution and we find that it is essential for the model to perform valid derendering on real images with our training setup.

Recognition tasks improve derendering quality (Rows 6-8). Removing recognition tasks from the multi-task training mixture notably reduces overall performance across all evaluation datasets, particularly impacting accuracy which reflects the model's semantic understanding ability. We hypothesize that the increase in F1 and drop in accuracy (such as the one observed on IMGUR5K) may be attributed to the model focusing less on the textual content and interpreting more background noise as strokes, which leads to digital inks that closely mimic the style of the input images, resulting in a higher likelihood of overlapping bounding boxes in F1 calculations.

Impact of frozen ViT in multi-task training. (Last row). Unfreezing the Vision Transformer (ViT) in multi-task training typically incurs training instability, as evidenced by increase in variance in model evaluations and an increased tendency to misinterpret background noise as textual content. Explaining the observed increase in F1 scores in Table 3 can be attributed to the model misinterpreting background noise as strokes, generating digital ink that visually closely resemble the input images, including the noise. This behavior results in a higher likelihood of overlapping bounding boxes, inflating F1 calculations. More details in Appendix E.1.

4.7 Limitations

We acknowledge the following two main limitations of our approach:

(1) Due to the limits in computational constraints and context length, it can derender only several characters or words in one model inference call;
(2) Consequently, it requires some form of segmentation of the handwritten page to run derendering on rather short individual segments (words in our implementation) and in the current form can not work on complex sketches or other objects with lots of strokes.

One thing that is **not** a limitation of our model is the use of OCR to provide the word labels – as shown in the first 2 rows of Table 2, the model performance degrades only slightly if the label is not provided or is inferred by the model. We also discuss some specific failure cases in Appendix J.

5 Conclusion

In this work we present the first approach to converting photos of handwriting into digital ink. We propose a training setup that works without paired training data, which can be difficult to acquire. We show that our method is robust to a variety of inputs, can work on full handwritten notes, and generalizes to out-of-domain sketches to some extent. Furthermore, our approach does not require complex modelling and can be constructed from standard building blocks. We release the weights and inference code of the Small-p model, with a subset of model-generated and human expert digital ink data. Future work may address the main limitations of our model stated above.

References

Notability Ink to Image conversion. `https://support.gingerlabs.com/hc/en-us/articles/5044440428570-Image-to-Ink-Conversion`, 2023. [Online; accessed 10-Jan-2024].

Hierarchical Text: Challenge on Unified OCR and Layout Analysis. `https://rrc.cvc.uab.es/?ch=18&com=tasks`, 2023. [Online; accessed 10-Jan-2024].

Google Cloud Vision Handwriting Text Detection API. `https://cloud.google.com/vision/docs/handwriting`, 2024. [Online; accessed 10-Jan-2024].

LiveScribe. `https://us.livescribe.com/`, 2024. [Online; accessed 10-Jan-2024].

NeoSmartPen. `https://neosmartpen.com/`, 2024. [Online; accessed 10-Jan-2024].

Rocketbook. `https://getrocketbook.com/`, 2024. [Online; accessed 10-Jan-2024].

Emre Aksan, Fabrizio Pece, and Otmar Hilliges. Deepwriting: Making digital ink editable via deep generative modeling. In *Proceedings of the 2018 CHI conference on human factors in computing systems*, pp. 1–14, 2018.

Jean-Baptiste Alayrac, Jeff Donahue, Pauline Luc, Antoine Miech, Iain Barr, Yana Hasson, Karel Lenc, Arthur Mensch, Katherine Millican, Malcolm Reynolds, et al. Flamingo: a visual language model for few-shot learning. *Advances in Neural Information Processing Systems*, 35:23716–23736, 2022.

Fakhraddin Alwajih, Eman Badr, and Sherif Abdou. Transformer-based models for arabic online handwriting recognition. *International Journal of Advanced Computer Science and Applications*, 13(5), 2022.

Taylor Archibald, Mason Poggemann, Aaron Chan, and Tony Martinez. Trace: a differentiable approach to line-level stroke recovery for offline handwritten text. In *Document Analysis and Recognition–ICDAR 2021: 16th International Conference, Lausanne, Switzerland, September 5–10, 2021, Proceedings, Part III 16*, pp. 414–429. Springer, 2021.

Emmanuel Augustin, Matthieu Carré, Emmanuèle Grosicki, J-M Brodin, Edouard Geoffrois, and Françoise Prêteux. Rimes evaluation campaign for handwritten mail processing. In *International Workshop on Frontiers in Handwriting Recognition (IWFHR'06),*, pp. 231–235, 2006.

Ayan Kumar Bhunia, Abir Bhowmick, Ankan Kumar Bhunia, Aishik Konwer, Prithaj Banerjee, Partha Pratim Roy, and Umapada Pal. Handwriting trajectory recovery using end-to-end deep encoder-decoder network. In *2018 24th International Conference on Pattern Recognition (ICPR)*, pp. 3639–3644. IEEE, 2018.

Ayan Kumar Bhunia, Pinaki Nath Chowdhury, Yongxin Yang, Timothy M Hospedales, Tao Xiang, and Yi-Zhe Song. Vectorization and rasterization: Self-supervised learning for sketch and handwriting. In *Proceedings of the IEEE/CVF Conference on Computer Vision and Pattern Recognition*, pp. 5672–5681, 2021.

James Bradbury, Roy Frostig, Peter Hawkins, Matthew James Johnson, Chris Leary, Dougal Maclaurin, George Necula, Adam Paszke, Jake VanderPlas, Skye Wanderman-Milne, et al. Jax: composable transformations of python+ numpy programs. 2018.

Chungkwong Chan. Stroke extraction for offline handwritten mathematical expression recognition. *IEEE Access*, 8:61565–61575, 2020.

Xi Chen, Xiao Wang, Soravit Changpinyo, AJ Piergiovanni, Piotr Padlewski, Daniel Salz, Sebastian Goodman, Adam Grycner, Basil Mustafa, Lucas Beyer, et al. Pali: A jointly-scaled multilingual language-image model. *arXiv preprint arXiv:2209.06794*, 2022a.

Xi Chen, Josip Djolonga, Piotr Padlewski, Basil Mustafa, Soravit Changpinyo, Jialin Wu, Carlos Riquelme Ruiz, Sebastian Goodman, Xiao Wang, Yi Tay, et al. Pali-x: On scaling up a multilingual vision and language model. *arXiv preprint arXiv:2305.18565*, 2023a.

Xi Chen, Xiao Wang, Lucas Beyer, Alexander Kolesnikov, Jialin Wu, Paul Voigtlaender, Basil Mustafa, Sebastian Goodman, Ibrahim Alabdulmohsin, Piotr Padlewski, et al. Pali-3 vision language models: Smaller, faster, stronger. *arXiv preprint arXiv:2310.09199*, 2023b.

Zhounan Chen, Daihui Yang, Jinglin Liang, Xinwu Liu, Yuyi Wang, Zhenghua Peng, and Shuangping Huang. Complex handwriting trajectory recovery: Evaluation metrics and algorithm. In *Proceedings of the asian conference on computer vision*, pp. 1060–1076, 2022b.

Jia Deng, Wei Dong, Richard Socher, Li-Jia Li, Kai Li, and Li Fei-Fei. Imagenet: A large-scale hierarchical image database. In *2009 IEEE conference on computer vision and pattern recognition*, pp. 248–255. Ieee, 2009.

David Doermann, Nathan Intrator, E Rivin, and Tal Steinherz. Hidden loop recovery for handwriting recognition. In *Proceedings Eighth International Workshop on Frontiers in Handwriting Recognition*, pp. 375–380. IEEE, 2002.

Alexey Dosovitskiy, Lucas Beyer, Alexander Kolesnikov, Dirk Weissenborn, Xiaohua Zhai, Thomas Unterthiner, Mostafa Dehghani, Matthias Minderer, Georg Heigold, Sylvain Gelly, Jakob Uszkoreit, and Neil Houlsby. An image is worth 16x16 words: Transformers for image recognition at scale. In *International Conference on Learning Representations*, 2021.

David Etter, Stephen Rawls, Cameron Carpenter, and Gregory Sell. A synthetic recipe for ocr. In *2019 International Conference on Document Analysis and Recognition (ICDAR)*, pp. 864–869, 2019. doi: 10.1109/ICDAR.2019.00143.

Emmanuèle Grosicki, Matthieu Carré, Jean-Marie Brodin, and Edouard Geoffrois. Results of the rimes evaluation campaign for handwritten mail processing. In *2009 10th International Conference on Document Analysis and Recognition*, pp. 941–945. IEEE, 2009.

Jonathan Heek, Anselm Levskaya, Avital Oliver, Marvin Ritter, Bertrand Rondepierre, Andreas Steiner, and Marc van Zee. Flax: A neural network library and ecosystem for JAX, 2023. URL `http://github.com/google/flax`.

Stefan Jager. Recovering writing traces in off-line handwriting recognition: Using a global optimization technique. In *Proceedings of 13th international conference on pattern recognition*, volume 3, pp. 150–154. IEEE, 1996.

Yoshiharu Kato and Makoto Yasuhara. Recovery of drawing order from single-stroke handwriting images. *IEEE Transactions on Pattern Analysis and Machine Intelligence*, 22(9):938–949, 2000.

Praveen Krishnan, Rama Kovvuri, Guan Pang, Boris Vassilev, and Tal Hassner. Textstylebrush: Transfer of text aesthetics from a single example. *IEEE Transactions on Pattern Analysis and Machine Intelligence*, 2023.

P Lallican, Christian Viard-Gaudin, and Stefan Knerr. From off-line to on-line handwriting recognition. In *EPRINTS-BOOK-TITLE*. 2004.

Yunyang Li, Lianwen Jin, Xinghua Zhu, and Teng Long. Scut-couch2008: A comprehensive online unconstrained chinese handwriting dataset. *ICFHR*, 2008:165–170, 2008.

Cheng-Lin Liu, Fei Yin, Da-Han Wang, and Qiu-Feng Wang. Casia online and offline chinese handwriting databases. In *2011 international conference on document analysis and recognition*, pp. 37–41. IEEE, 2011.

M. Liwicki and H. Bunke. Iam-ondb - an on-line english sentence database acquired from handwritten text on a whiteboard. In *Eighth International Conference on Document Analysis and Recognition (ICDAR'05)*, pp. 956–961 Vol. 2, 2005. doi: 10.1109/ICDAR.2005.132.

Shangbang Long, Siyang Qin, Dmitry Panteleev, Alessandro Bissacco, Yasuhisa Fujii, and Michalis Raptis. Towards end-to-end unified scene text detection and layout analysis. In *Proceedings of the IEEE/CVF Conference on Computer Vision and Pattern Recognition*, pp. 1049–1059, 2022.

Shangbang Long, Siyang Qin, Dmitry Panteleev, Alessandro Bissacco, Yasuhisa Fujii, and Michalis Raptis. Icdar 2023 competition on hierarchical text detection and recognition. *arXiv preprint arXiv:2305.09750*, 2023.

U-V Marti and Horst Bunke. A full english sentence database for off-line handwriting recognition. In *Proceedings of the Fifth International Conference on Document Analysis and Recognition. ICDAR'99 (Cat. No. PR00318)*, pp. 705–708. IEEE, 1999.

Margaret Mitchell, Simone Wu, Andrew Zaldivar, Parker Barnes, Lucy Vasserman, Ben Hutchinson, Elena Spitzer, Inioluwa Deborah Raji, and Timnit Gebru. Model cards for model reporting. In *Proceedings of the conference on fairness, accountability, and transparency*, pp. 220–229, 2019.

Haoran Mo, Edgar Simo-Serra, Chengying Gao, Changqing Zou, and Ruomei Wang. General virtual sketching framework for vector line art. *ACM Transactions on Graphics (TOG)*, 40(4):1–14, 2021.

Elmokhtar Mohamed Moussa, Thibault Lelore, and Harold Mouchère. Set, sort! a novel sub-stroke level transformers for offline handwriting to online conversion. In *International Conference on Document Analysis and Recognition*, pp. 81–97. Springer, 2023.

Michael Murdock, Shawn Reid, Blaine Hamilton, and Jackson Reese. Icdar 2015 competition on text line detection in historical documents. In *2015 13th international conference on document analysis and recognition (ICDAR)*, pp. 1171–1175. IEEE, 2015.

Hung Tuan Nguyen, Cuong Tuan Nguyen, and Masaki Nakagawa. Icfhr 2018–competition on vietnamese online handwritten text recognition using hands-vnondb (vohtr2018). In *2018 16th International Conference on Frontiers in Handwriting Recognition (ICFHR)*, pp. 494–499. IEEE, 2018.

Hung Tuan Nguyen, Tsubasa Nakamura, Cuong Tuan Nguyen, and Masaki Nakawaga. Online trajectory recovery from offline handwritten japanese kanji characters of multiple strokes. In *2020 25th International Conference on Pattern Recognition (ICPR)*, pp. 8320–8327. IEEE, 2021.

Reza Pourreza, Apratim Bhattacharyya, Sunny Panchal, Mingu Lee, Pulkit Madan, and Roland Memisevic. Painter: Teaching auto-regressive language models to draw sketches. In *Proceedings of the IEEE/CVF International Conference on Computer Vision (ICCV) Workshops*, pp. 305–314, October 2023.

Yu Qiao, Mikihiko Nishiara, and Makoto Yasuhara. A framework toward restoration of writing order from single-stroked handwriting image. *IEEE transactions on pattern analysis and machine intelligence*, 28(11): 1724–1737, 2006.

Adam Roberts, Hyung Won Chung, Gaurav Mishra, Anselm Levskaya, James Bradbury, Daniel Andor, Sharan Narang, Brian Lester, Colin Gaffney, Afroz Mohiuddin, et al. Scaling up models and data with t5x and seqio. *Journal of Machine Learning Research*, 24(377):1–8, 2023.

Paul K Rubenstein, Chulayuth Asawaroengchai, Duc Dung Nguyen, Ankur Bapna, Zalán Borsos, Félix de Chaumont Quitry, Peter Chen, Dalia El Badawy, Wei Han, Eugene Kharitonov, et al. Audiopalm: A large language model that can speak and listen. *arXiv preprint arXiv:2306.12925*, 2023.

Patsorn Sangkloy, Nathan Burnell, Cusuh Ham, and James Hays. The sketchy database: learning to retrieve badly drawn bunnies. *ACM Transactions on Graphics (TOG)*, 35(4):1–12, 2016.

Noam Shazeer and Mitchell Stern. Adafactor: Adaptive learning rates with sublinear memory cost. In *International Conference on Machine Learning*, pp. 4596–4604. PMLR, 2018.

Arti Shivram, Chetan Ramaiah, Srirangaraj Setlur, and Venu Govindaraju. Ibm_ub_1: A dual mode unconstrained english handwriting dataset. In *2013 12th International Conference on Document Analysis and Recognition*, pp. 13–17. IEEE, 2013.

Taichi Sumi, Brian Kenji Iwana, Hideaki Hayashi, and Seiichi Uchida. Modality conversion of handwritten patterns by cross variational autoencoders. In *2019 international conference on document analysis and recognition (ICDAR)*, pp. 407–412. IEEE, 2019.

Chen Sun, Abhinav Shrivastava, Saurabh Singh, and Abhinav Gupta. Revisiting unreasonable effectiveness of data in deep learning era. In *Proceedings of the IEEE international conference on computer vision*, pp. 843–852, 2017.

Ashish Vaswani, Noam Shazeer, Niki Parmar, Jakob Uszkoreit, Llion Jones, Aidan N Gomez, Łukasz Kaiser, and Illia Polosukhin. Attention is all you need. *Advances in neural information processing systems*, 30, 2017.

Christian Viard-Gaudin, Pierre Michel Lallican, Stefan Knerr, and Philippe Binter. The ireste on/off (ironoff) dual handwriting database. In *Proceedings of the Fifth International Conference on Document Analysis and Recognition. ICDAR'99 (Cat. No. PR00318)*, pp. 455–458. IEEE, 1999.

Christian Viard-Gaudin, Pierre-Michel Lallican, and Stefan Knerr. Recognition-directed recovering of temporal information from handwriting images. *Pattern Recognition Letters*, 26(16):2537–2548, 2005.

Yael Vinker, Ehsan Pajouheshgar, Jessica Y Bo, Roman Christian Bachmann, Amit Haim Bermano, Daniel Cohen-Or, Amir Zamir, and Ariel Shamir. Clipasso: Semantically-aware object sketching. *ACM Transactions on Graphics (TOG)*, 41(4):1–11, 2022.

Mahes Visvalingam and J Duncan Whyatt. The douglas-peucker algorithm for line simplification: re-evaluation through visualization. In *Computer graphics forum*, volume 9, pp. 213–225. Wiley Online Library, 1990.

Jiarui Xu, Xingyi Zhou, Shen Yan, Xiuye Gu, Anurag Arnab, Chen Sun, Xiaolong Wang, and Cordelia Schmid. Pixel-aligned language model. In *Proceedings of the IEEE/CVF Conference on Computer Vision and Pattern Recognition*, pp. 13030–13039, 2024.

Linting Xue, Noah Constant, Adam Roberts, Mihir Kale, Rami Al-Rfou, Aditya Siddhant, Aditya Barua, and Colin Raffel. mT5: A massively multilingual pre-trained text-to-text transformer. In Kristina Toutanova, Anna Rumshisky, Luke Zettlemoyer, Dilek Hakkani-Tur, Iz Beltagy, Steven Bethard, Ryan Cotterell, Tanmoy Chakraborty, and Yichao Zhou (eds.), *Proceedings of the 2021 Conference of the North American Chapter of the Association for Computational Linguistics: Human Language Technologies*, pp. 483–498, Online, June 2021. Association for Computational Linguistics. doi: 10.18653/v1/2021.naacl-main.41. URL `https://aclanthology.org/2021.naacl-main.41`.

Xiaohua Zhai, Xiao Wang, Basil Mustafa, Andreas Steiner, Daniel Keysers, Alexander Kolesnikov, and Lucas Beyer. Lit: Zero-shot transfer with locked-image text tuning. In *Proceedings of the IEEE/CVF Conference on Computer Vision and Pattern Recognition*, pp. 18123–18133, 2022.

Xiong Zhang, Min Wang, Lijuan Wang, Qiang Huo, and Haifeng Li. Building handwriting recognizers by leveraging skeletons of both offline and online samples. In *2015 13th International Conference on Document Analysis and Recognition (ICDAR)*, pp. 406–410. IEEE, 2015.

A Appendix

Outline of Appendix

1. **Full-page Results** (Appendix B)
2. **Data Statistics and Preprocessing** (Appendix C)
3. **Survey of Derendering Models** (Appendix D)
4. **Further Details of Ablation Studies** (Appendix E)
5. **Rendering and Data Augmentation** (Appendix F)
6. **Additional Model Details** (Appendix G)
7. **General Virtual Sketching Framework Performance** (Appendix H)
8. **Online Handwriting Recognizer Details** (Appendix I)
9. **Failure Cases** (Appendix J)
10. **Human Evaluation** (Appendix K)
11. **Model Card** (Appendix L)
12. **Additional Visualizations** (Appendix M)
13. **Impact Statements** (Appendix N)

B Full-page Results

We show the full-page results on samples that resemble real-life inputs (mostly from Unsplash with keyword search for "handwriting", and others collected by the authors with consent from the writers) produced by three variants of our models.

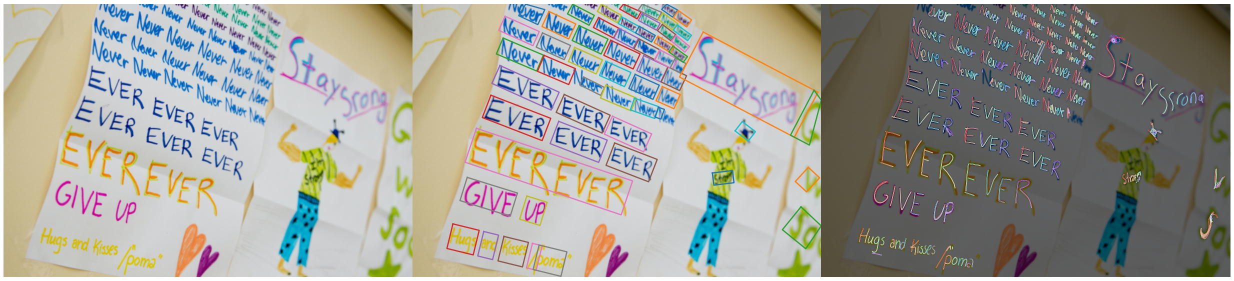

Figure 11: **Large-i** full page results of handwritten notes in a real-life scenario, credit: Unsplash.

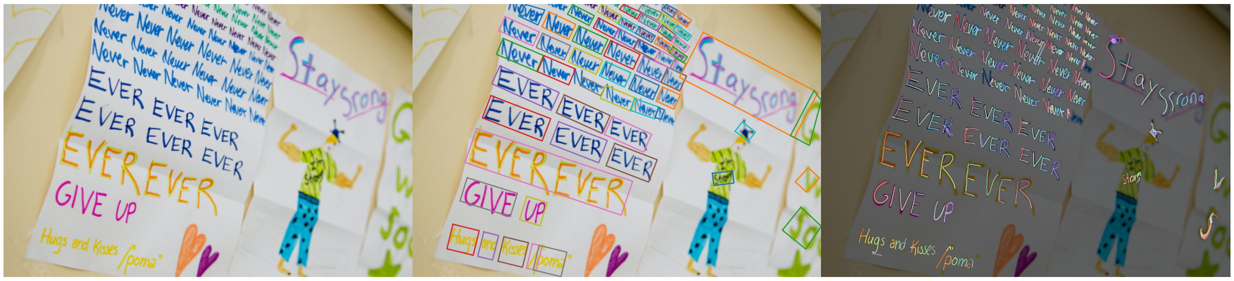

Figure 12: **Small-i** full page results of handwritten notes in a real-life scenario, credit: Unsplash.

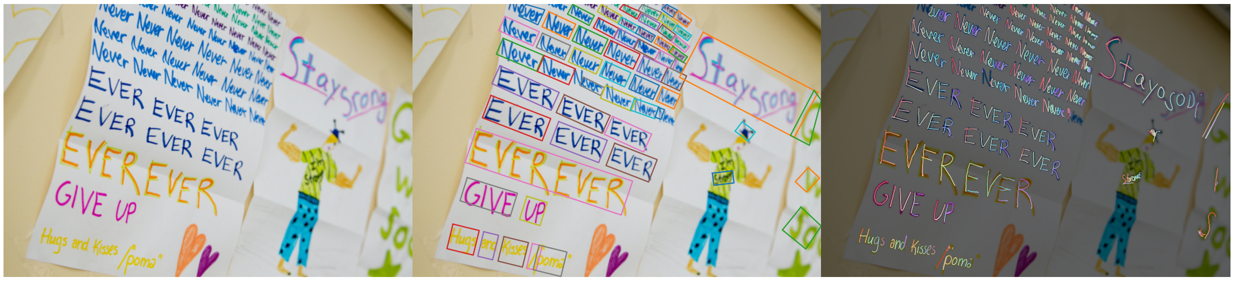

Figure 13: **Small-p** full page results of handwritten notes in a real-life scenario, credit: Unsplash.

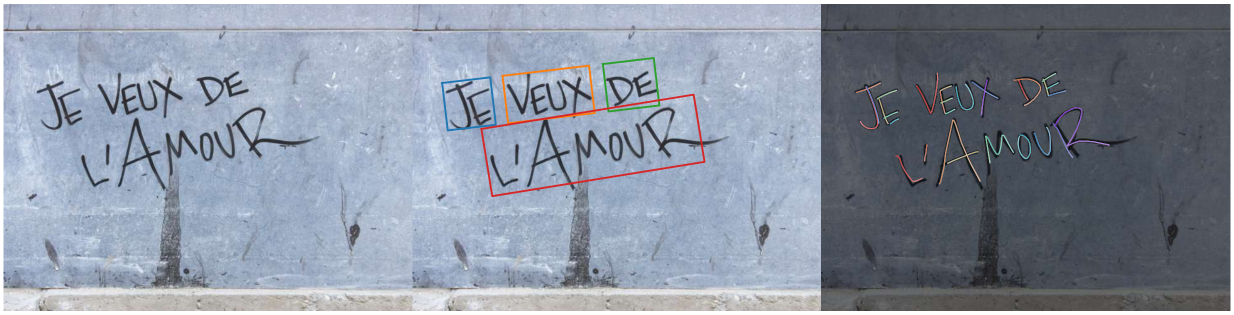

Figure 14: **Large-i** full page results of French sample. credit: Unsplash

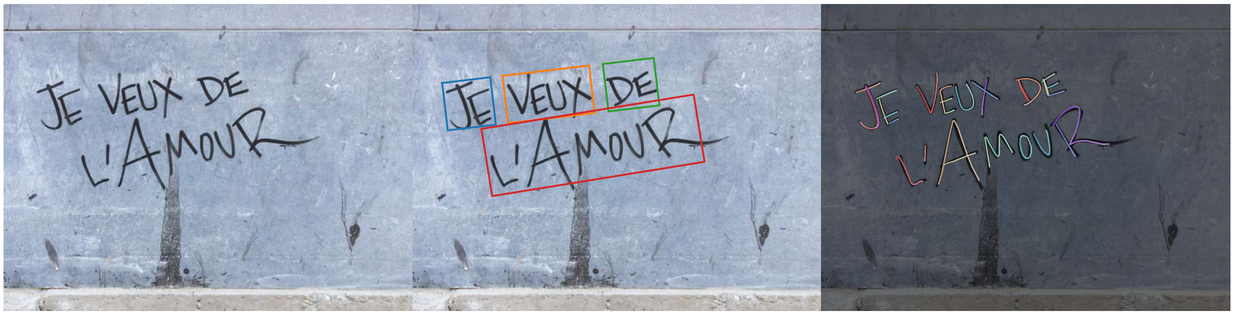

Figure 15: **Small-i** full page results of French sample. credit: Unsplash

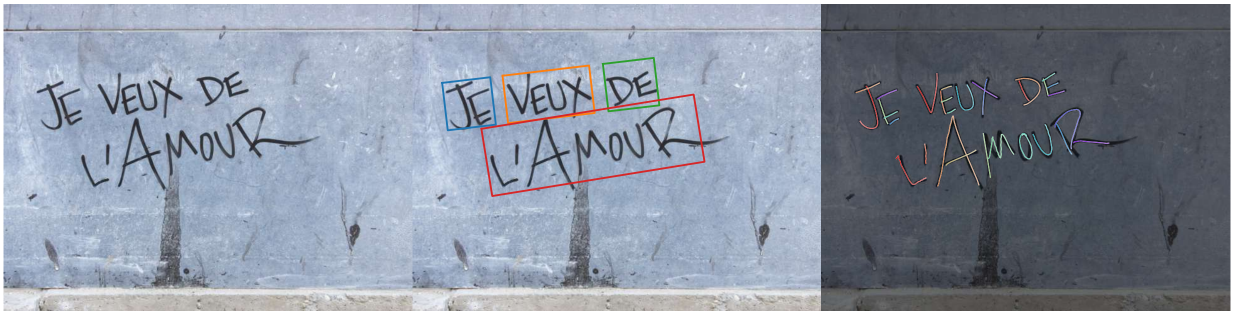

Figure 16: **Small-p** full page results of French sample. credit: Unsplash

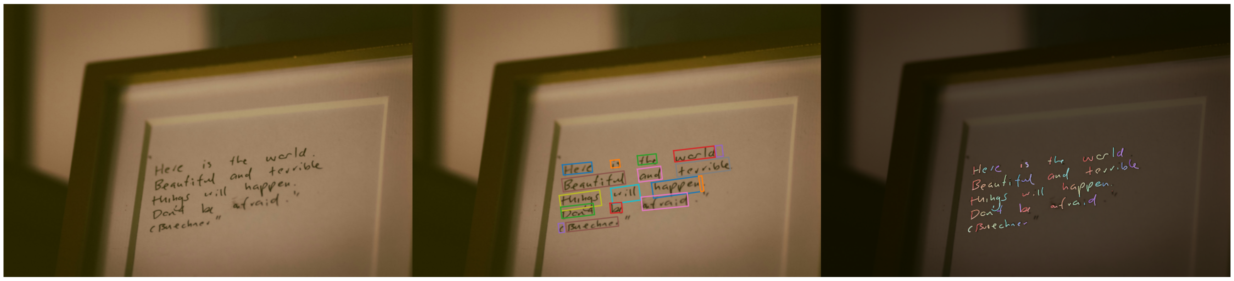

Figure 17: **Large-i** full page results of handwritten notes in a real-life scenario with low resolution, credit: Unsplash.

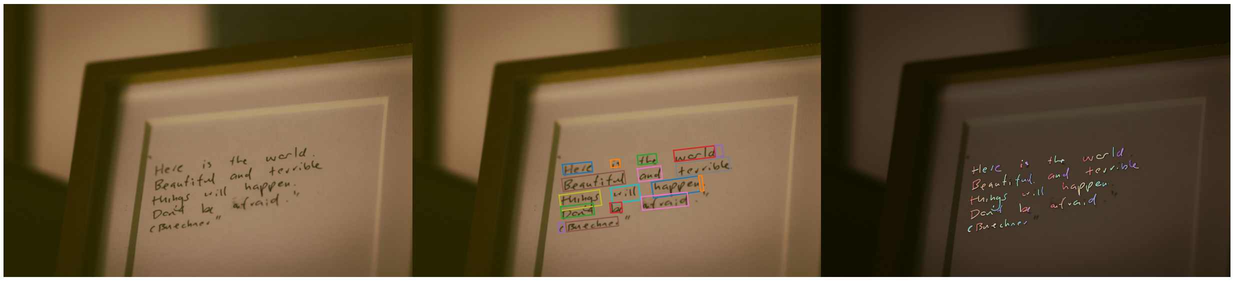

Figure 18: **Small-i** full page results of handwritten notes in a real-life scenario with low resolution, credit: Unsplash.

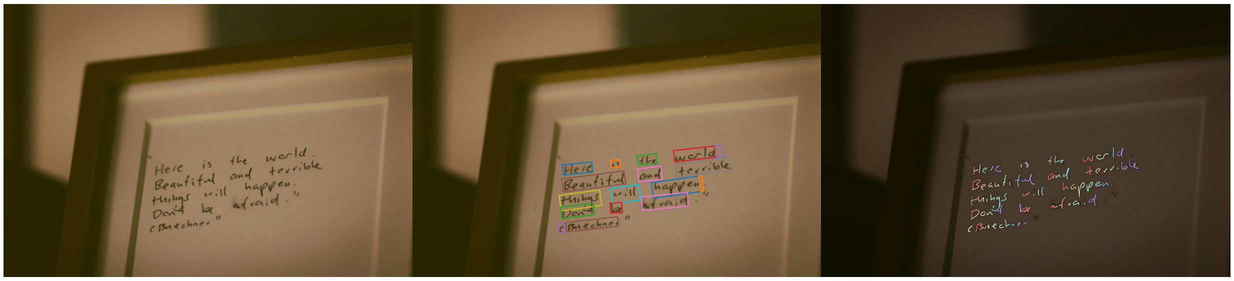

Figure 19: **Small-p** full page results of handwritten notes in a real-life scenario with low resolution, credit: Unsplash.

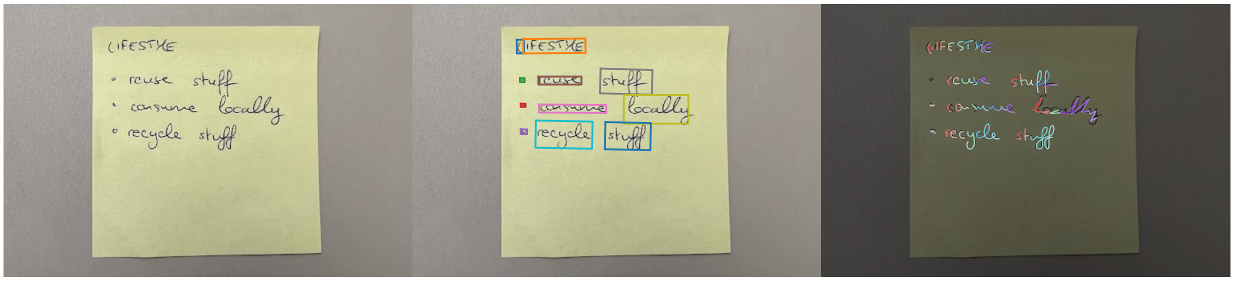

Figure 20: **Large-i** full page results of a Post-It note.

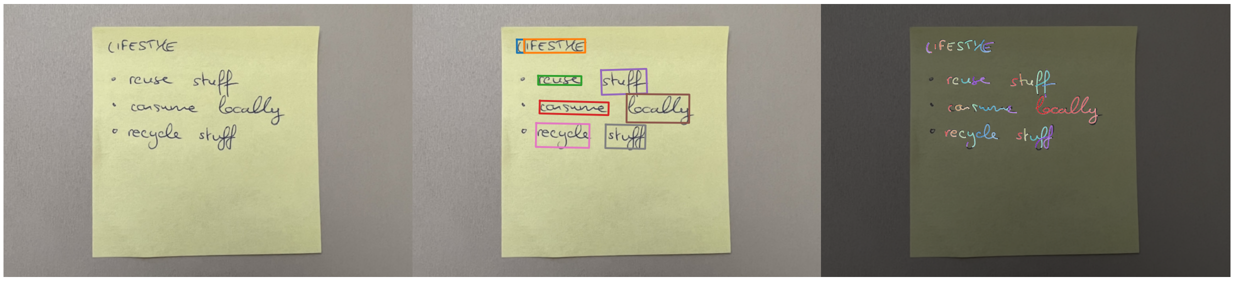

Figure 21: **Small-i** full page results of a Post-It note.

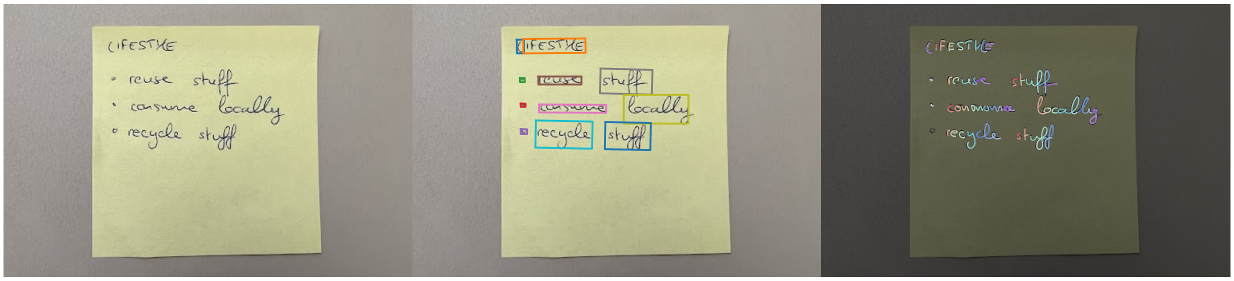

Figure 22: **Small-p** full page results of a Post-It note.

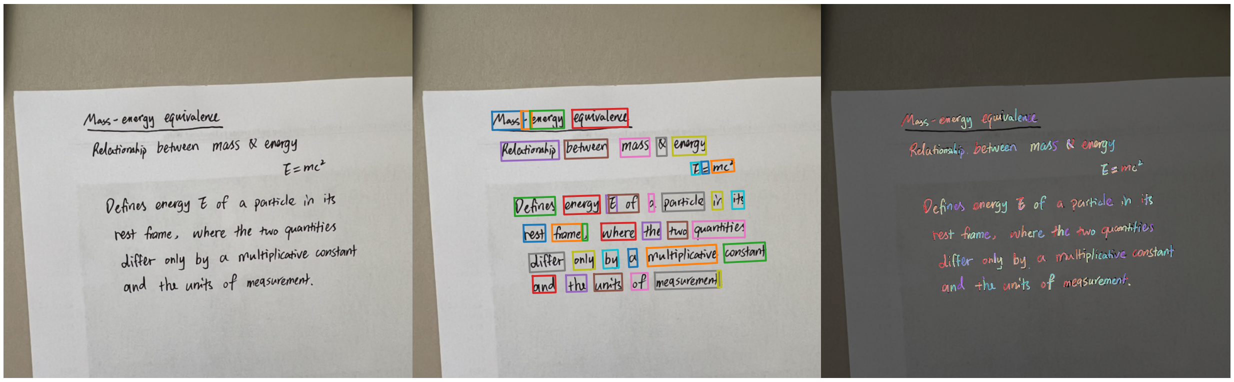
Mass - energy equivalence
Relationship between mass & energy
E = mc²
Defines energy E of a particle in its
rest frame, where the two quantities
differ only by a multiplicative constant
and the units of measurement.

Figure 23: **Large-i** full page results of handwritten notes of mass-energy equivalence.

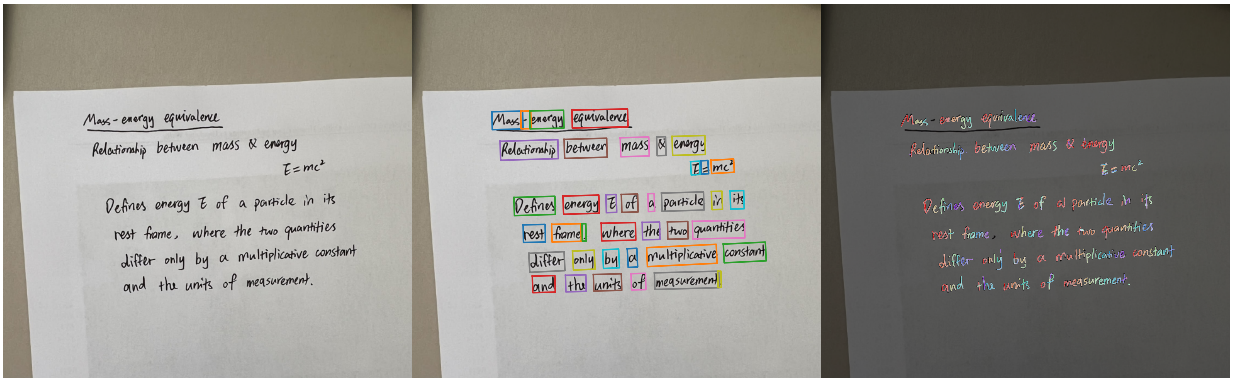
Mass - energy equivalence
Relationship between mass & energy
E = mc²
Defines energy E of a particle in its
rest frame, where the two quantities
differ only by a multiplicative constant
and the units of measurement.

Figure 24: **Small-i** full page results of handwritten notes of mass-energy equivalence.

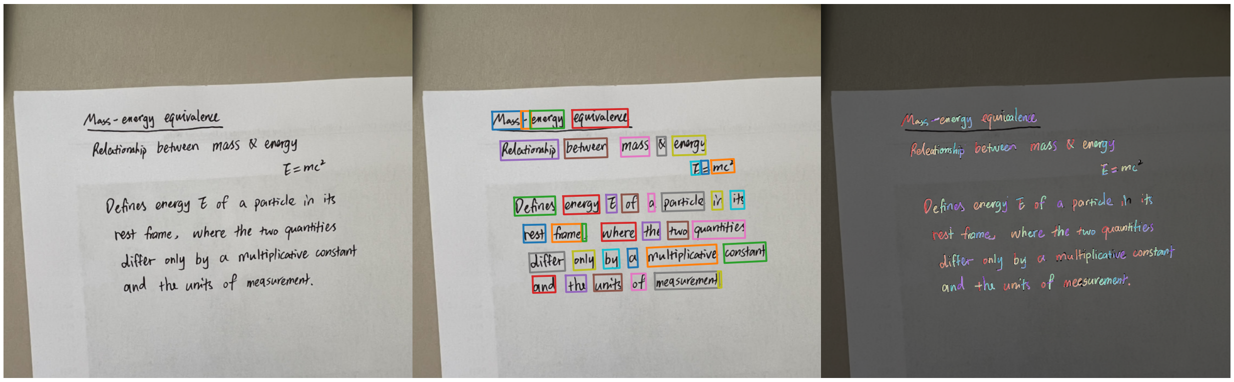
Mass - energy equivalence
Relationship between mass & energy
E = mc²
Defines energy E of a particle in its
rest frame, where the two quantities
differ only by a multiplicative constant
and the units of measurement.

Figure 25: **Small-p** full page results of handwritten notes of mass-energy equivalence.

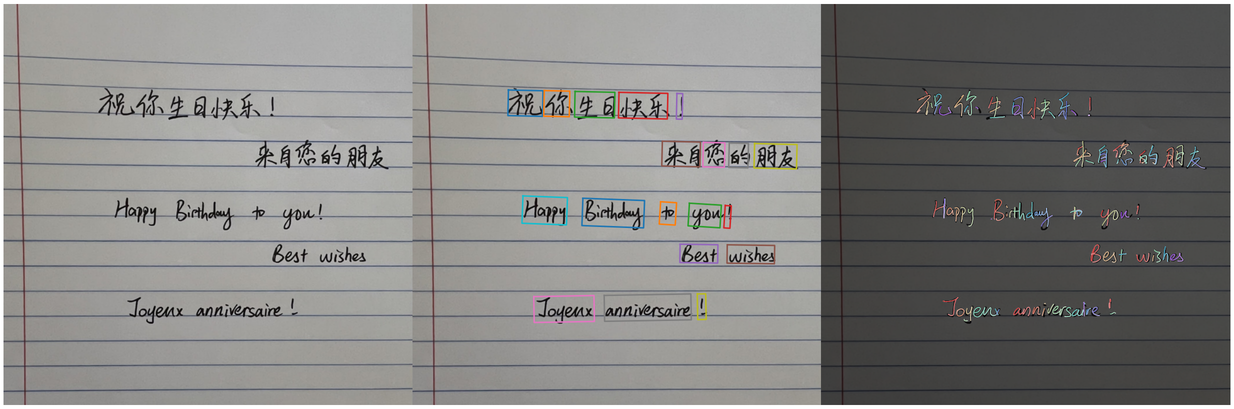

Figure 26: **Large-i** full page results of multilingual handwritten notes.

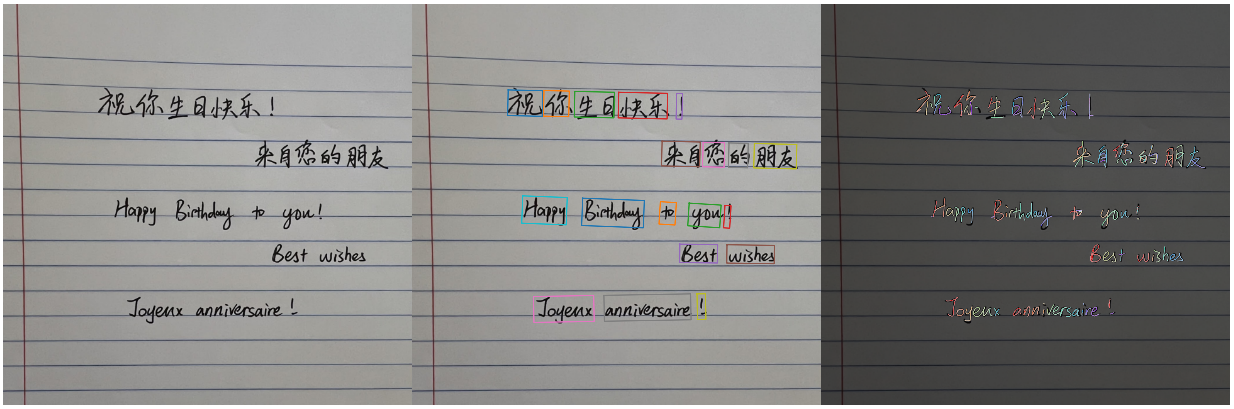

Figure 27: **Small-i** full page results of multilingual handwritten notes.

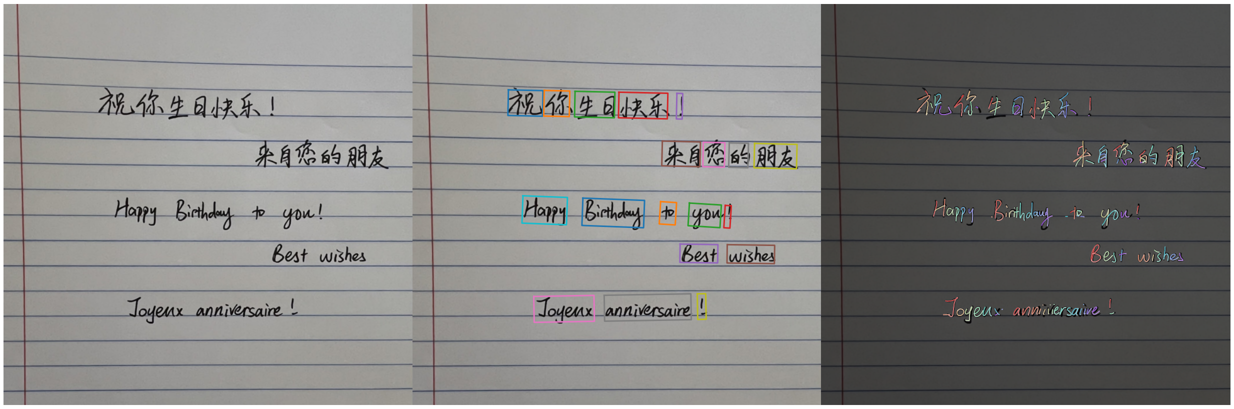

Figure 28: **Small-p** full page results of multilingual handwritten notes.

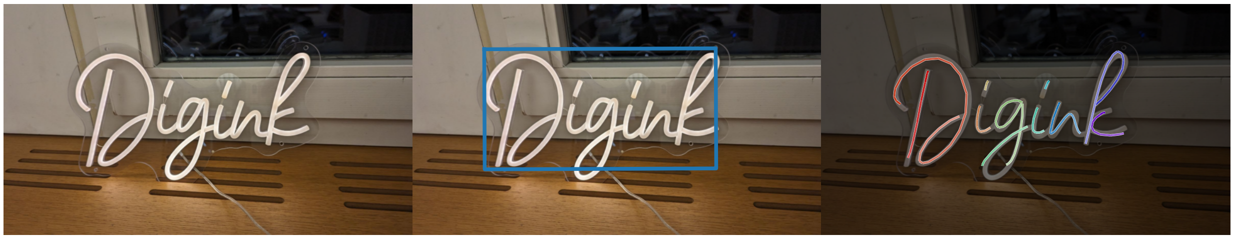

Figure 29: **Large-i** full page results of OOD sample.

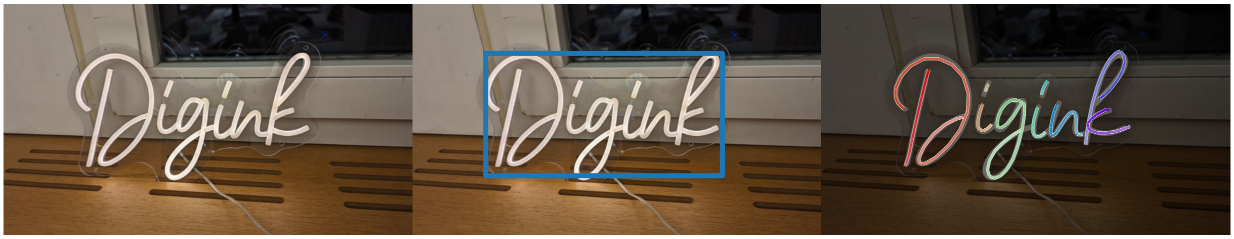

Figure 30: **Small-i** full page results of OOD sample.

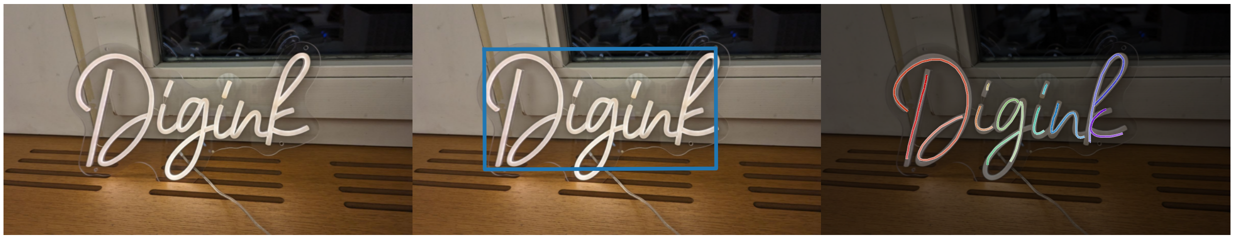

Figure 31: **Small-p** full page results of OOD sample.

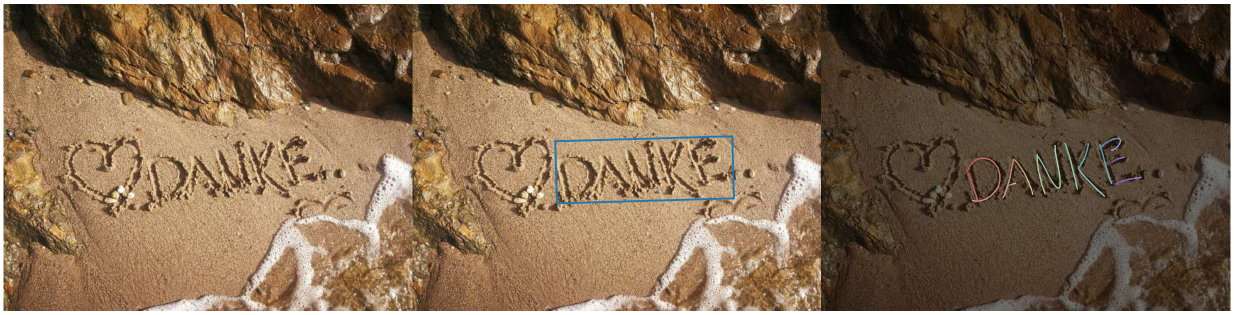

Figure 32: **Large-i** full page results of OOD sample, credit: Unsplash.

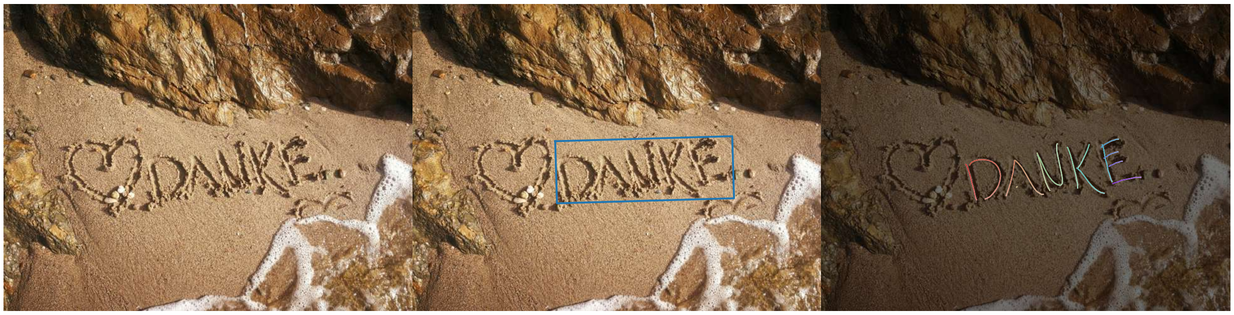

Figure 33: **Small-i** full page results of OOD sample, credit: Unsplash.

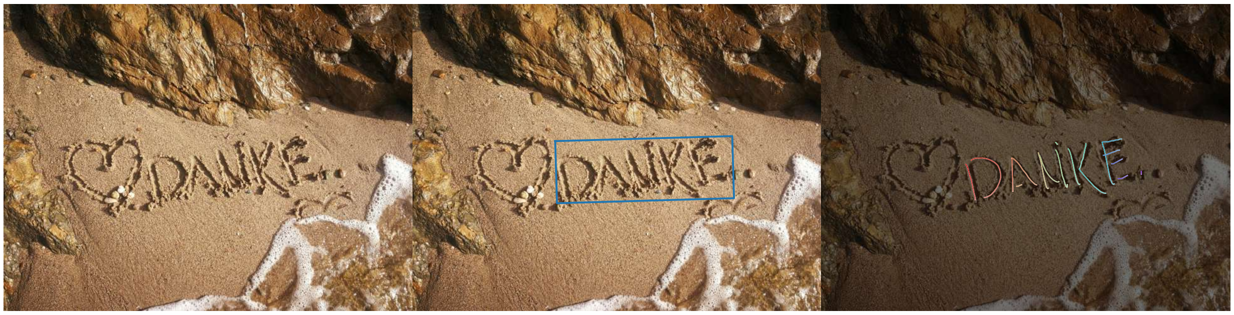

Figure 34: **Small-p** full page results of OOD sample, credit: Unsplash.

C Data statistics and Preprocessing

We present the language distribution of the digital ink datasets used to train our in-house (**-i** suffix) and publicly available (**-p** suffix) models in Figures 35 and 36, datasets and corresponding number of samples used in training our public model in Table 4. The in-house OCR dataset comprises of approximately 500k samples, and in-house Digital Ink dataset comprises of approximately 16M samples.

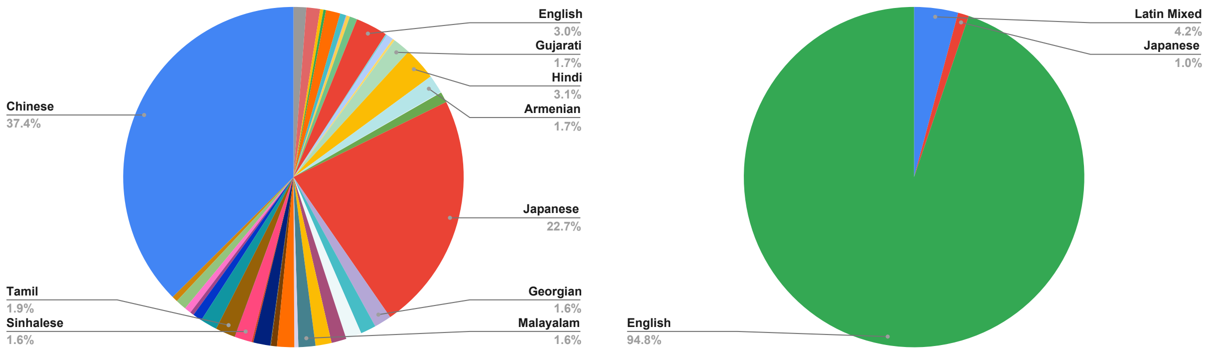

Figure 35: In-house Datasets Language Distributions. **Left:** Digital inks, **Right:** OCR for Recognition. These datasets are used to train both in-house models **Small-i** and **Large-i**.

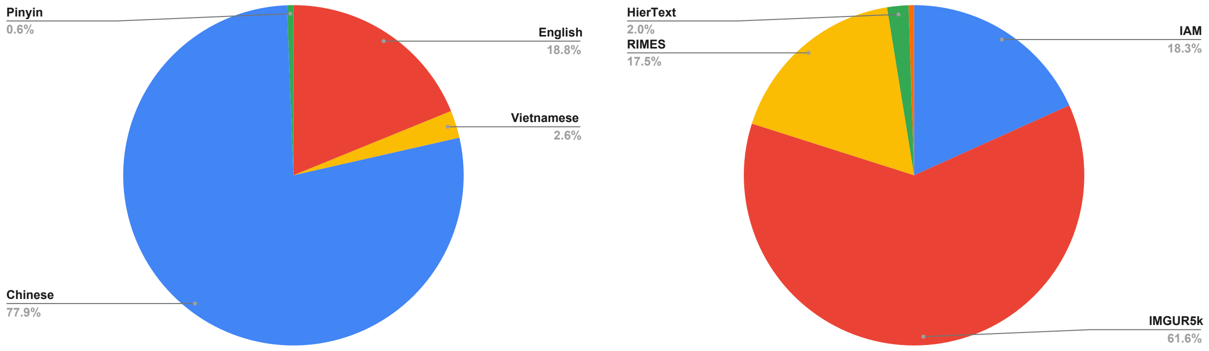

Figure 36: Public Datasets. Language distribution of public Digital ink datasets used to train our public models (on the left) and public OCR datasets used to train our public available model **Small-p** (on the right).

D Survey of Derendering Models

In this section we provide a small survey of recent published pen trajectory recovery approaches and show that none of them release sufficient materials to reproduce their work with a reasonable amount of effort. We illustrate this with Table 5.

Table 4: Public training datasets used for training **small-p**.

Task Type	Dataset	Samples	License
Derendering	DeepWriting (words)	89,565	Custom[1]
	DeepWriting (lines)	33,933	Custom[1]
	DeepWriting (characters)	359,643	Custom[1]
	VNOnDB	66,991	MIT[2]
	SCUT-COUCH (chars)	1,998,784	Custom[3]
	SCUT-COUCH (pinyin)	15,653	Custom[3]
Recognition	IAM word-level (train)	53,839	Custom[4]
	IMGUR5k (train)	181,792	CC BY-NC[5]
	RIMES word-level (train)	51,738	CC BY-NC[5]
	HierText (train)	5,978	CC BY-SA[6]
	ICDAR-2015 (train)	1,535	Custom[7]

Custom license (CC BY-NC-SA 4.0 + non-distribution). See: URL.
MIT License. See: URL.
Custom license (research-only, attribution). See: URL.
Custom license (research-only, non-commercial, attribution). See: URL.
CC BY-NC 4.0. See: URL.
CC BY-SA 4.0. See: URL.
Custom license (research-only, attribution). See: URL.

Table 5: Existing pen trajectory recovery approaches and their reproducibility.

Study	Code Availability	Data Availability	Model Weights Availability	Year
Mohamed Moussa et al. (2023)	✗	✓	✗	2023
Chen et al. (2022b)	✗ Repo missing core elements: data preprocessing, incompatible configs	✓	✗	2022
Archibald et al. (2021)	✗	✓	✗	2021
Bhunia et al. (2021)	✗ Repo missing core elements: training scripts, data preprocessing	✓	✗	2021
Nguyen et al. (2021)	✗	✓	✗	2021
Sumi et al. (2019)	✗	✓	✗	2019
Bhunia et al. (2018)	✓	✗	✗	2018

E Further Details of Ablation Studies

E.1 Frozen ViT helps training stability

We investigated the impact of freezing the vision encoder during training on model stability and derendering performance. To assess training stability, we analyzed the ratio of empty ink predictions across training steps on the "golden" human traced dataset (detailed in Section 4.5.1). Empty inks typically occur when the model confuses tasks, mistakenly outputting text instead of ink or both (different tasks depicted in Figure 3). Our analysis revealed significantly greater variance between runs with an unfrozen setup compared to the consistent learning observed with a frozen vision encoder (Figure 37).

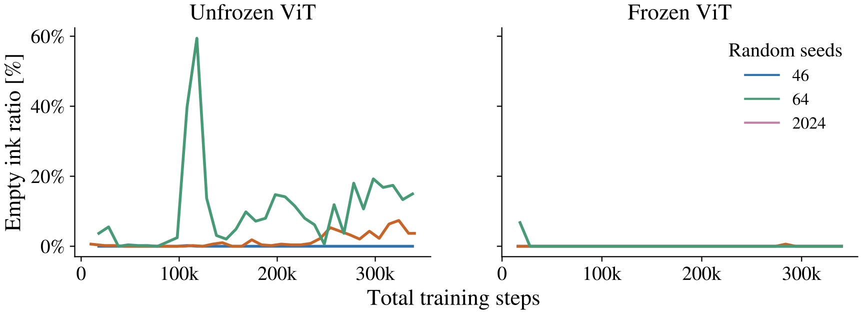

Figure 37: **Comparison between frozen and unfrozen ViT Small-i trainings.** Comparison is executed with 3 random seeds. **Left:** ratio of empty ink outputs for unfrozen ViT multi-task training setup. **Right:** ratio of empty ink outputs for the frozen ViT multi-task training setup, both use inference task *Derender with Text*.

Furthermore, in terms of final model derendering performance, we identified that certain model initializations (controlled by seeds) within the unfrozen setup could also converge to functional models with comparable abilities to those trained with a frozen setup. These models demonstrate superior preservation of visual ink details but exhibit increased sensitivity to background noise. We present a visual comparison of their output characteristics in Figure 38.

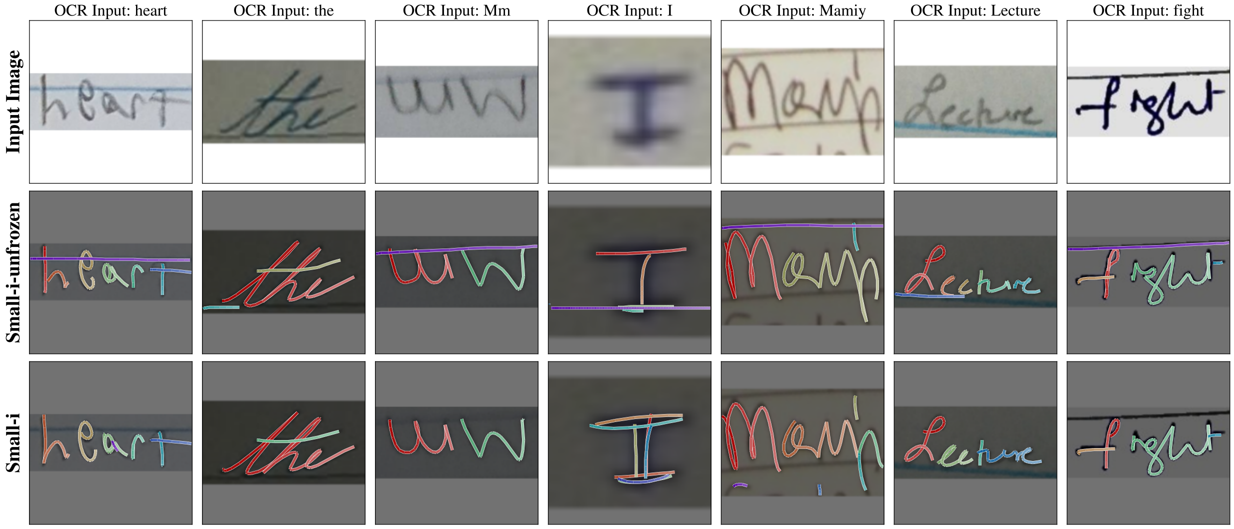

Figure 38: Difference between **Small-i-unfrozen** which was trained with an unfrozen ViT (seed 46 in Figure 37) and **Small-i** which was trained with a frozen ViT. This shows that **Small-i-unfrozen** is more sensitive to background noise compared to **Small-i**.

E.2 Inference type matters

As we first illustrated in Section 4.6, different inference tasks can produce different output digital inks especially when the input image of text is semantically or geometrically ambiguous due to either image quality or how the texts were written. For example the first column of Figure 39 where the word "wich" is removed by the writer with a strike through line but still recognized by both *Recognize and Derender* (model intrinsic) and *Derender with Text* (extrinsic OCR system) inference, and the difference in understanding and locating the textual information in input image results in different output digital inks. Additionally, the output from *Vanilla Derender* where semantics are not intentionally involved during training is more robust to ambiguous inputs but shows poorer semantic consistency with the input image.

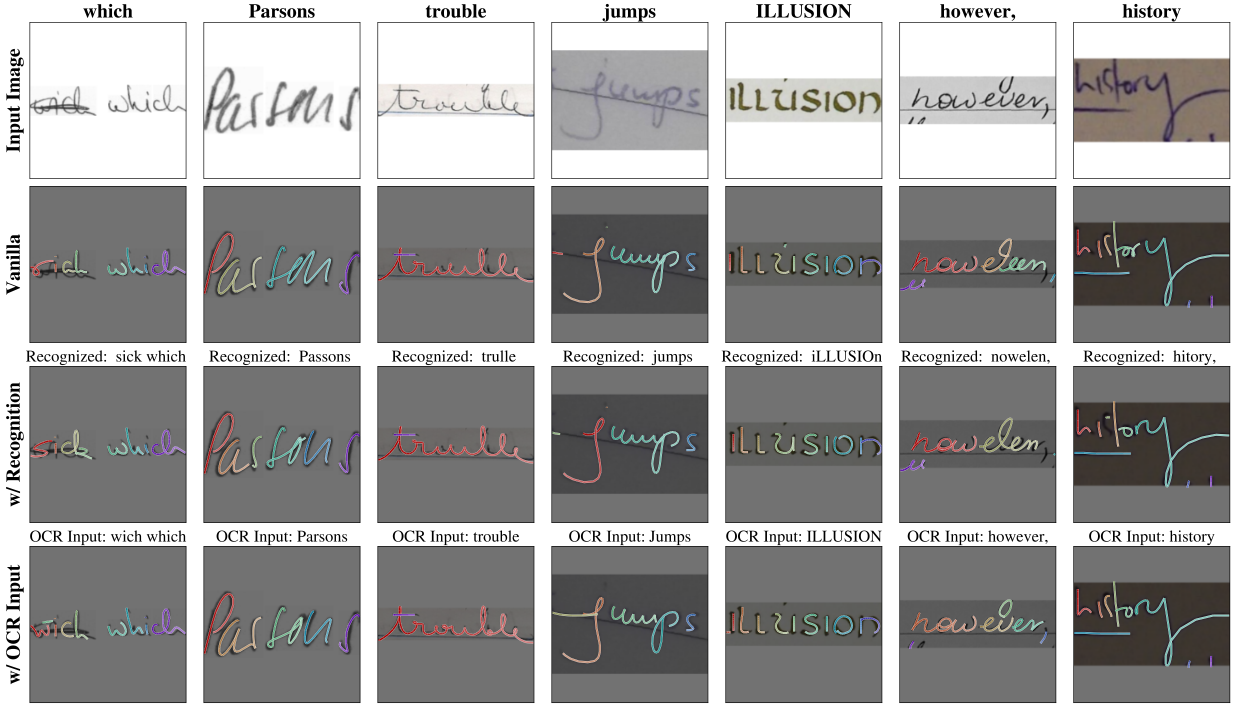

Figure 39: **Difference between inference tasks** of **Small-i** on samples from 3 public evaluation datasets, where the texts on top are the ground truth labels for the images in these datasets. **Vanilla** stands for inference with *Vanilla Derendering*, **w/Recognition** stands for inference with *Recognize and Derender*, and **w/ OCR Input** stands for inference with *Derender with Text* where we resort to an OCR system.

For *Derender with Text* inference, we have shown that how external textual input could benefit the model's semantic understanding. We explore the behavior of the model in cases where the external text is different than the ground-truth textual information in Figure 40. The results reveal that the model's output is not solely determined by input text. It demonstrates the ability to produce valid outputs even when external textual information is incomplete or erroneous.

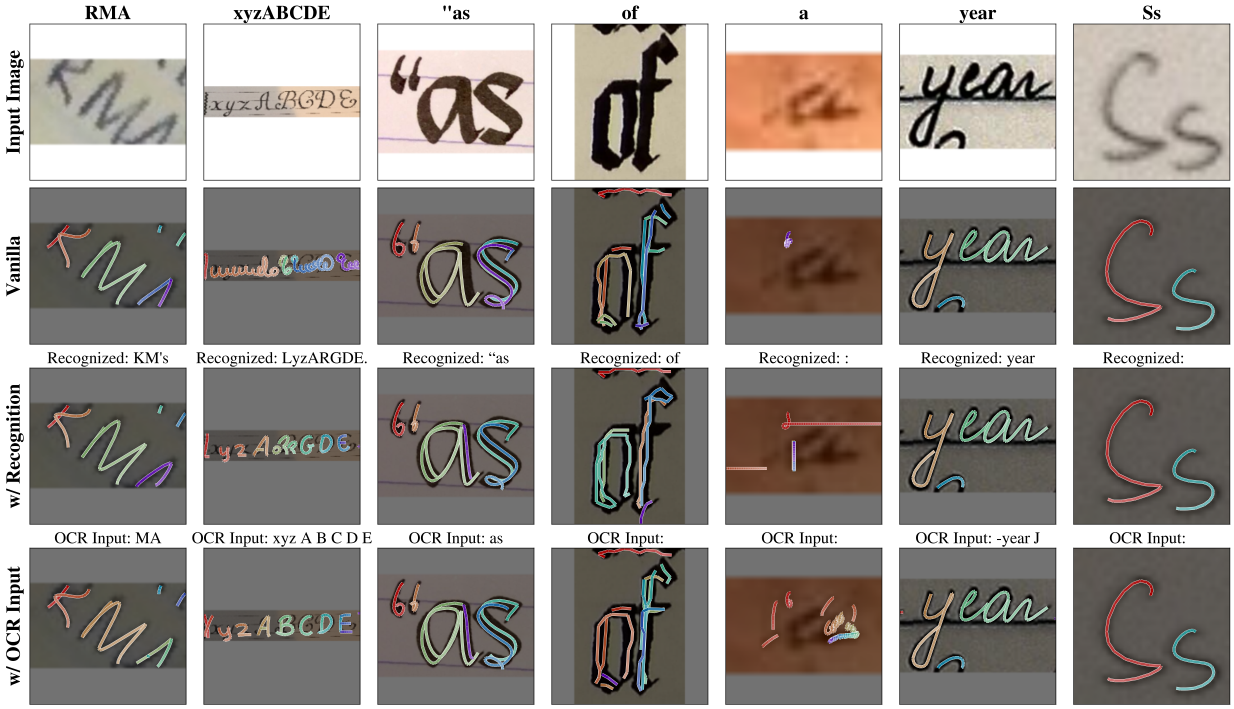

Figure 40: **Cases when there is a mismatch between ground-truth textual information and external textual information provided to the model.** We evaluated this using **Small-i** on samples from 3 public evaluation datasets, where the texts on top are the ground truth labels for the images in these datasets. **Vanilla** stands for inference with *Vanilla Derender*, **w/Recognition** stands for inference with *Recognize and Derender*, and **w/ OCR Input** stands for inference with *Derender with Text* where we resort to an OCR system.

F Rendering and Data Augmentation

To create synthetic rendered inks of our online samples, we use the Cairo graphics library to render online ink samples onto a 224 × 224 canvas. We then add several augmentations to rendered samples.

Before rendering, we first randomly rotate the samples. Then, we pick the color of the strokes and the background uniformly at random from the RGB color space and render the ink with a random width. Furthermore, we add lines, grids, or Gaussian noise into the background with a fixed probability. Finally, we potentially add box blur on the resulting image. This approach was mainly inspired by approaches from synthetic OCR generation, e.g. as described in (Etter et al., 2019). The detailed parameters of data augmentation and some samples are shown in Table 6. An example of how samples augmented with all parameters chosen at random could appear in the training set can be seen in Figure 41. Other approaches, such as perspective skew, shifting, scaling, or padding, did not show any improvements in the model performance and were discarded.

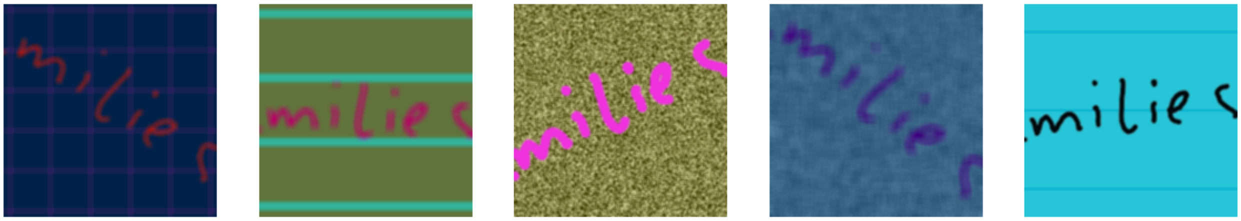

Figure 41: Demonstration of possible ways to combine all used augmentations. (Sample from (Aksan et al., 2018))

Table 6: Data Augmentations Overview (sample from Aksan et al. 2018).

Augmentation	**Possible Values**	**Examples**
Rotation	angle (rad): $[-\frac{\pi}{4}, \frac{\pi}{4}]$	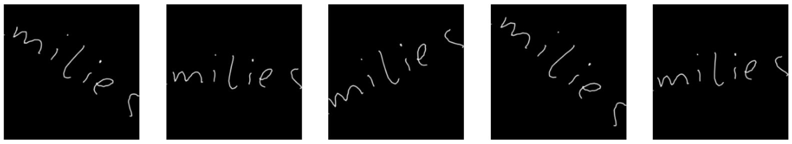
Stroke color	RGB: $[0, 1]^3$	
Background color	RGB: $[0, 1]^3$	
Stroke Width	width: $[1\text{px}, 12\text{px}]$	
Lines	line width: $[1\text{px}, 6\text{px}]$ line dist: $[10\text{px}, 100\text{px}]$ line color: RGB: $[0, 1]^3$	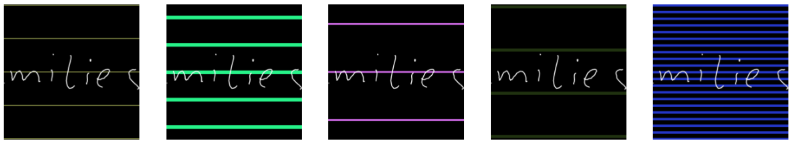
Grids	line width: $[1\text{px}, 6\text{px}]$ line dist: $[10\text{px}, 100\text{px}]$ line color: RGB: $[0, 1]^3$	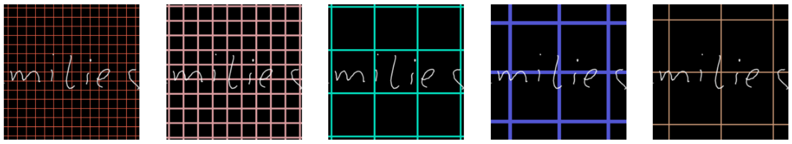
Gaussian Noise	standard dev.: $[50, 500]$	
Box blur	radius: $[0\text{px}, 5\text{px}]$	

G Additional Model Details

The overview and individual components of three versions of our model **Small-i**, **Small-p**, and **Large-i** is shown in Table 7.

Table 7: Model overview and components.

Model	Components	Parameters	Training Data
Large-i	ViT-L mT5-Large	303M 783M	In-house proprietary datasets as shown in Appendix C.
Small-i	ViT-B mT5-Base	85M 247M	In-house proprietary datasets as shown in Appendix C.
Small-p	ViT-B mT5-Base	85M 247M	Publicly available datasets as shown in Appendix C.

Implementation Details. Similar to PaLI models (Chen et al., 2022a; 2023a;b), our models together with the training mixtures are implemented in `JAX/Flax` (Bradbury et al., 2018) using the open-source `T5X`, `SeqIO` (Roberts et al., 2023) and `Flaxformer` (Heek et al., 2023) frameworks. For training, we use the Adafactor optimizer (Shazeer & Stern, 2018) with $\beta_1 = 0$, second order moment of 0.8, and a language-model–style teacher forcing with softmax cross-entropy loss. For the learning rate schedule, we use the linear decay scheduler with a peak learning rate of 0.01, 5k steps of warmup and a linear decay with decay factor of $3e-6$, and a dropout of 0.1 on both ViT encoder and the mT5 encoder-decoder. We train our models for 340k steps with batch size 512. With frozen ViT encoders, the training of a 340M parameter model (such as **Small-i** or **Small-p**) takes ∼33h on 64 TPU v5e chips and the training of a 1B parameter **Large-i** model takes ∼105h on 64 TPU v5e chips, both run on an internal TPU v5e cluster and should be reproducible with public GCP TPU v5e. Inference with a 340M parameter model takes around 1 hour for all 3 datasets, and 3 hours with **Large-i**.

Compute. For the results reported in Table 3, we train one 340M parameter model per ablation. For entries with estimated variances, we train each model with 3 different seeds, respectively. This totals in ∼330h on 64 TPU v5e chips of training. We additionally train **Small-p** and **Large-i** to obtain the results in Table 2, accounting for ∼138h on 64 TPU v5e chips. In total, all experiments in this paper require a total of ∼500h of compute for training the models and running inference.

Decoding. In our experiments, we observe marginal performance improvements in derendering tasks through adjustments in temperature sampling. However, for the sake of reproducibility and framework simplicity, we employ a greedy decoding strategy during inference for all tasks, with model checkpoints selected from the final step.

Training Mixture. As described in Section 3.2, the training mixture consists of 5 tasks constructed using SeqIO (Roberts et al., 2023). These tasks are pre-shuffled before training, ensuring each task appears with equal probability throughout the entire training process. And to foster reproducibility, the input pipeline as well as the model initialization are designed to be deterministic, reducing randomness-induced variations that could affect our design choices.

H General Virtual Sketching (Mo et al., 2021) Framework Performance

We demonstrate the performance of three GVS models from the official GitHub repository: Line Drawing Vectorization, Rough Sketch Simplification, and Photo to Line Drawing Conversion in two setups (original image as input and binarized image as input) in Figure 42. We inspect the samples visually on the more challenging HierText dataset. The photo to line drawing model was trained on people portrait photos and fails to generalize to the images of text. Binarization is beneficial for both remaining setups and reduces the noise when derendering texts. Line Drawing Vectorization and Sketch Simplification perform similarly on the inspected samples, we choose Line Drawing Vectorization on binarized images as a baseline since this model was trained on black & white raster images and therefore treats binarized samples as in-domain. For derendering of the sketches (Figure 7) we use the Sketch Simplification model as intended by the authors.

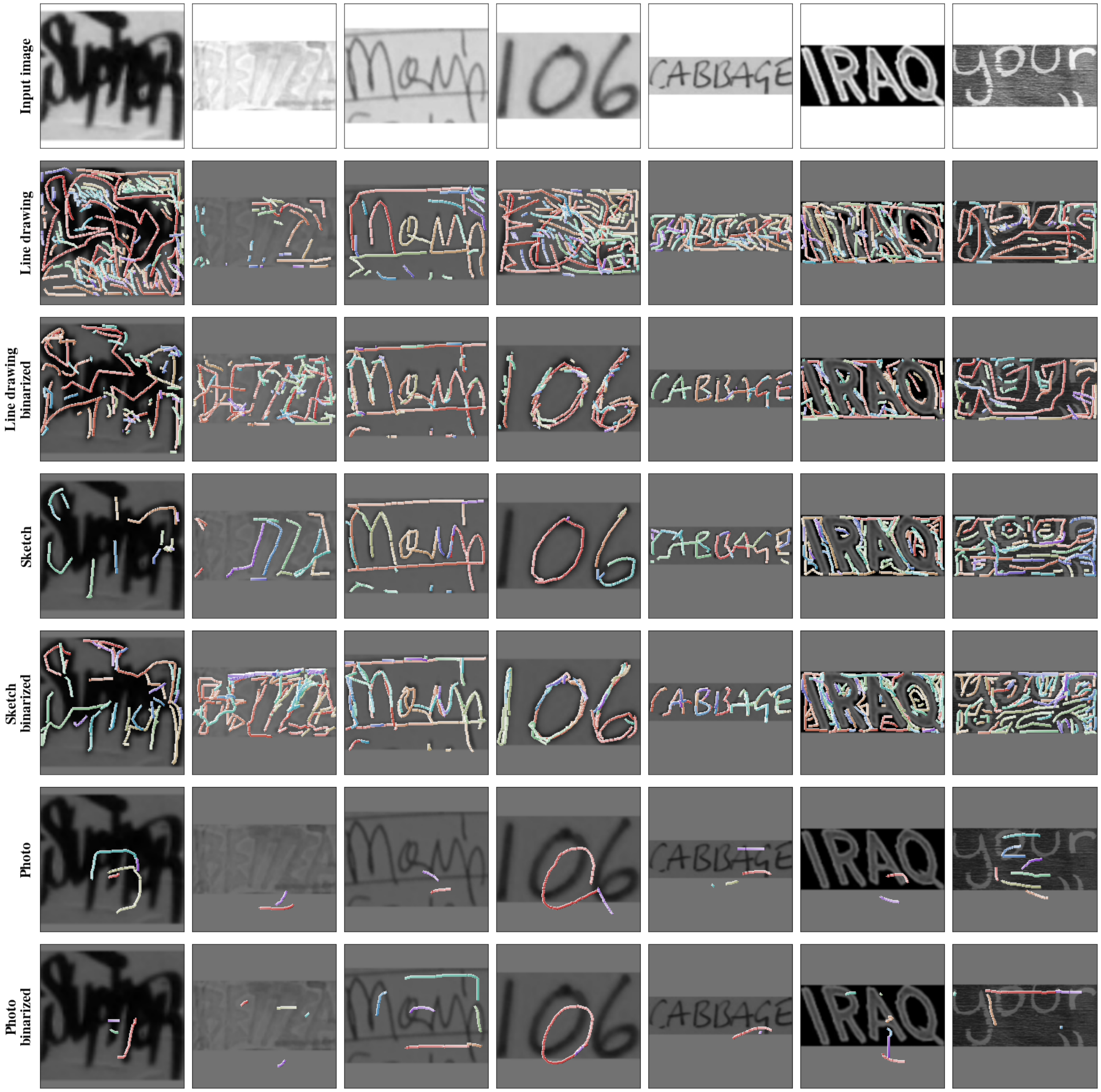

Figure 42: Comparison between General Virtual Sketching Framework inference setups.

I Online Handwriting Recognizer Details

In this section we provide the result of online handwriting recognizers used to evaluate the low-level feature similarity of real inks for IAMOnDB dataset and inks derendered by **Small-p**, **Small-i** and **Large-i** (see Table 8). We observe that the inks acquired with all of our models perform similarly when used as training data both on their own and in combination with real digital inks.

Table 8: Online handwriting recognition results on IAMOnDB test set for models trained on real digital inks (IAMOnDB train set), derendered digital inks (from IAM train set) and the combination of the two.

	IAMOnDB	**Small-i IAM derendered**	**Small-i IAMOnDB + IAM derendered**	**Small-p IAM derendered**	**Small-p IAMOnDB + IAM derendered**	**Large-i IAM derendered**	**Large-i IAMOnDB + IAM derendered**
CER	6.1	7.8	4.6	8.2	**4.5**	8.4	4.6

Additionally, we describe the architecture and our recognition training procedure. We choose a common approach of training a (relatively small, 9.2M, due to the amount of the training data) Transformer encoder combined with a CTC loss, similar to Alwajih et al. 2022. We fix the same preprocessing steps for both real and derendered inks. Those include shifting and scaling the inks to start at the origin and have a fixed y side, time resampling at 20 ms for real inks and time hallucination (assuming the predicted ink tokens are produced at a fixed sampling rate of 20ms, matching the training data) and adding pen up strokes. We apply a random rotation within ±45° with probability 0.5 as data augmentation to account for the small size of the dataset. The points from the ink are encoded into Bezier curves. The input features are then processed by 7 transformer attention layers with 8 attention heads.

We train the models on a training set of IAMOnDB only (baseline), derendered IAM train set only and the combination of the two for 17.5k steps with batch size of 64. We perform a hyper-parameter search for dropout and learning rate on the same grid for all 3 setups. The best parameters for each model can be found in Table 9.

Table 9: Recognizer parameters found through hyper-parameter search.

Parameter	**IAMOnDB**	**Small-i IAM derendered**	**Small-i IAMOnDB + IAM derendered**	**Small-p IAM derendered**	**Small-p IAMOnDB + IAM derendered**	**Large-i IAM derendered**	**Large-i IAMOnDB + IAM derendered**
Dropout	0.25	0.25	0.3	0.3	0.25	0.25	0.25
Learning rate	0.005	0.001	0.001	0.005	0.005	0.001	0.001

J Failure Cases

While our system exhibits satisfactory performance across various tested inputs, we have identified specific failure patterns that warrant further attention. As some examples shown in the Figures 38 and 40 we notice model's performance deteriorates when processing samples with wider stroke widths or significant variations in stroke width. Additionally, we observed that the model's ability to preserve handwriting details improves with the scaling of the vision component (visualized in Figure 5, aligned with findings in Section 4.5.1). However, we also noticed a lack of proportional scaling between the vision (ViT) and text-ink (mT5) components negatively impacts semantic understanding.

Furthermore, our investigation, as detailed in Section 4.6, demonstrated that unfreezing the vision heads allows the model to capture more input image details. Nevertheless, this enhancement comes at the cost of training instability and increased confusion between textual information and background noise. Future research in this domain may explore fine-tuning the vision backbone while leveraging the existing semantic understanding of ink representations, following a similar idea as described in (Zhai et al., 2022).

K Human Evaluation

We provide the text of our evaluation instructions in Table 10 and the screenshot of the interface in Figure 43. Furthermore, we show the samples and corresponding rating (after majority voting) in Figure 44.

Table 10: Human evaluation campaign instructions.

Description	**Instruction**
Task setup	You will be looking at input images of photos of handwriting in a variety of styles and the corresponding digital ink tracing performed either by a human or by one of our derendering models. Each stroke is rendered in a different color and with color gradient (darker → whiter) to reflect the direction. You will see the derendered ink as well as the derendered ink overlaid on top of the image and can use either to make the judgment. For each sample answer the two questions on the right and click submit to proceed to the next sample.
Is Reasonable	Is the digital ink a reasonable tracing of the input image? • Yes, it's a good tracing • It's an okay tracing, but has some small errors • It's a bad tracing, has some major artifacts One interpretation of the quality of the ink could be like this: If you were to use it in a note taking app, would you • keep it as is: good tracing • need to make some edits: okay tracing • not use it at all: bad tracing If you need some examples to get a better feeling, you can use the ones below, however there is some ambiguity within the task since we don't want to impose any strict rules but allow for a natural variety of what people find a good derendering (it is designed to be subjective).
Is Real	Could this digital ink have been produced by a human? • Yes • No In this question go with your intuition, do you think the ink could have been traced by a [reasonable] human?

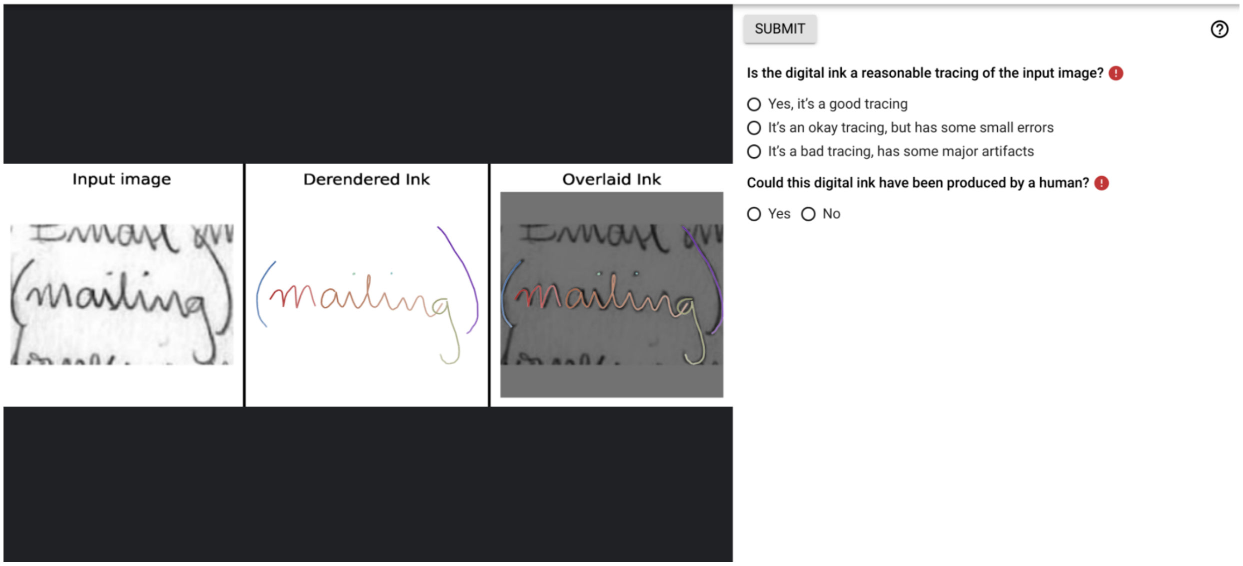

Is the digital ink a reasonable tracing of the input image?

○ Yes, it's a good tracing
○ It's an okay tracing, but has some small errors
○ It's a bad tracing, has some major artifacts

Could this digital ink have been produced by a human?

○ Yes ○ No

Figure 43: A screenshot of the human evaluation interface.

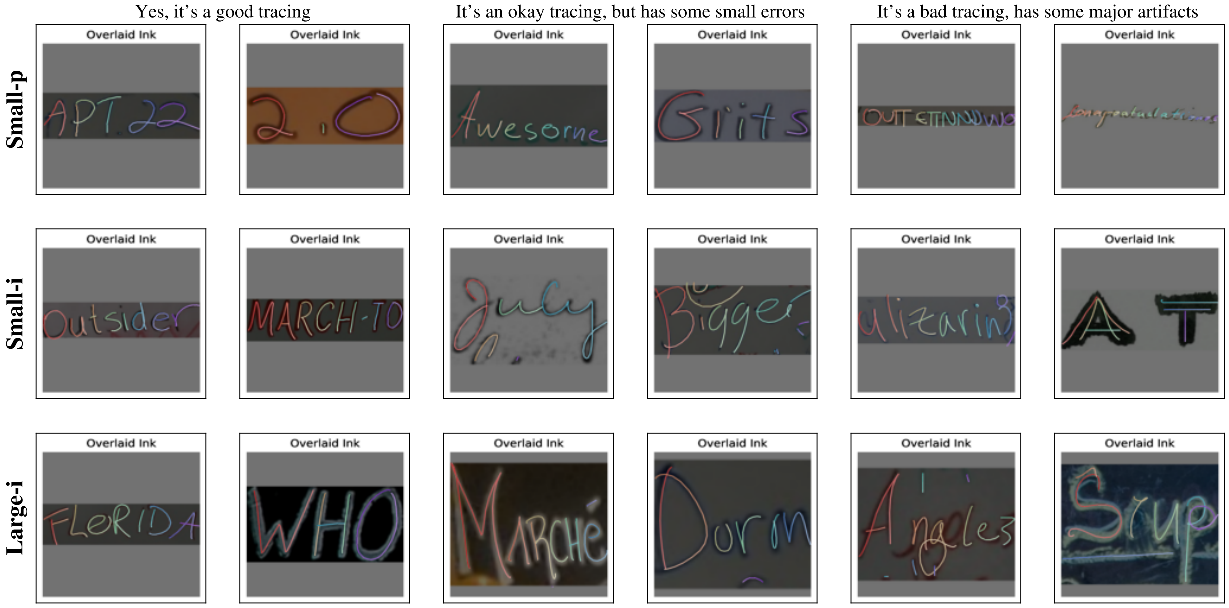
Yes, it's a good tracing
It's an okay tracing, but has some small errors
It's a bad tracing, has some major artifacts
Small-p
Small-i
Large-i
Overlaid Ink

Figure 44: Examples of samples produced by our models and ratings given to them by our evaluators.

L Model Card

We present the model card (Mitchell et al., 2019) of our public release model **Small-p** in Table 11.

Table 11: Model card of publicly available **Small-p**.

Model Summary	
Model Architecture	A multimodal sequence-to-sequence Transformer (Vaswani et al., 2017) model with the mT5 (Xue et al., 2021) encoder-decoder architecture. It takes text tokens and ViT (Dosovitskiy et al., 2021) dense image embeddings as inputs to an encoder and autoregressively predicts discrete text and ink tokens with a decoder.
Input(s)	A pair of image and text.
Output(s)	Generated digital ink.
Usage	
Application	The model is for research prototype, and the public version Small-p is planned to be released and available for the public.
Known Caveats	None.
System Type	
System Description	This is a standalone model.
Upstream Dependencies	None.
Downstream Dependencies	None.
Implementation Frameworks	
Hardware & Software	Hardware: TPU v5e. Software: T5X (Roberts et al., 2023), JAX/Flax (Bradbury et al., 2018), Flaxformer (Heek et al., 2023) For implementation details please refer to Appendix G.
Compute Requirements	Please refer to Appendix G.
Data Overview	
Training Datasets	The ViT encoder (Dosovitskiy et al., 2021) is pre-trained on ImageNet-21k (Deng et al., 2009), mT5 encoder and decoder are initialized from scratch. The entire model is trained on the mixture of publicly available datasets described in Appendix C.
Evaluation Results	
Evaluation Methods	Human evaluation (reported in Section 4.5.1) and automated evaluations (reported in Section 4.5.2).
Model Usage & Limitations	
Sensitive Use	The model is capable of converting images to digital inks. This model should not be used for any of the privacy intruding use cases, e.g. forging handwritings.
Known Limitations	Reported in Section 4.7.
Ethical Considerations & Potential Societal Consequences	Reported in Appendix N.

M Additional Visualizations

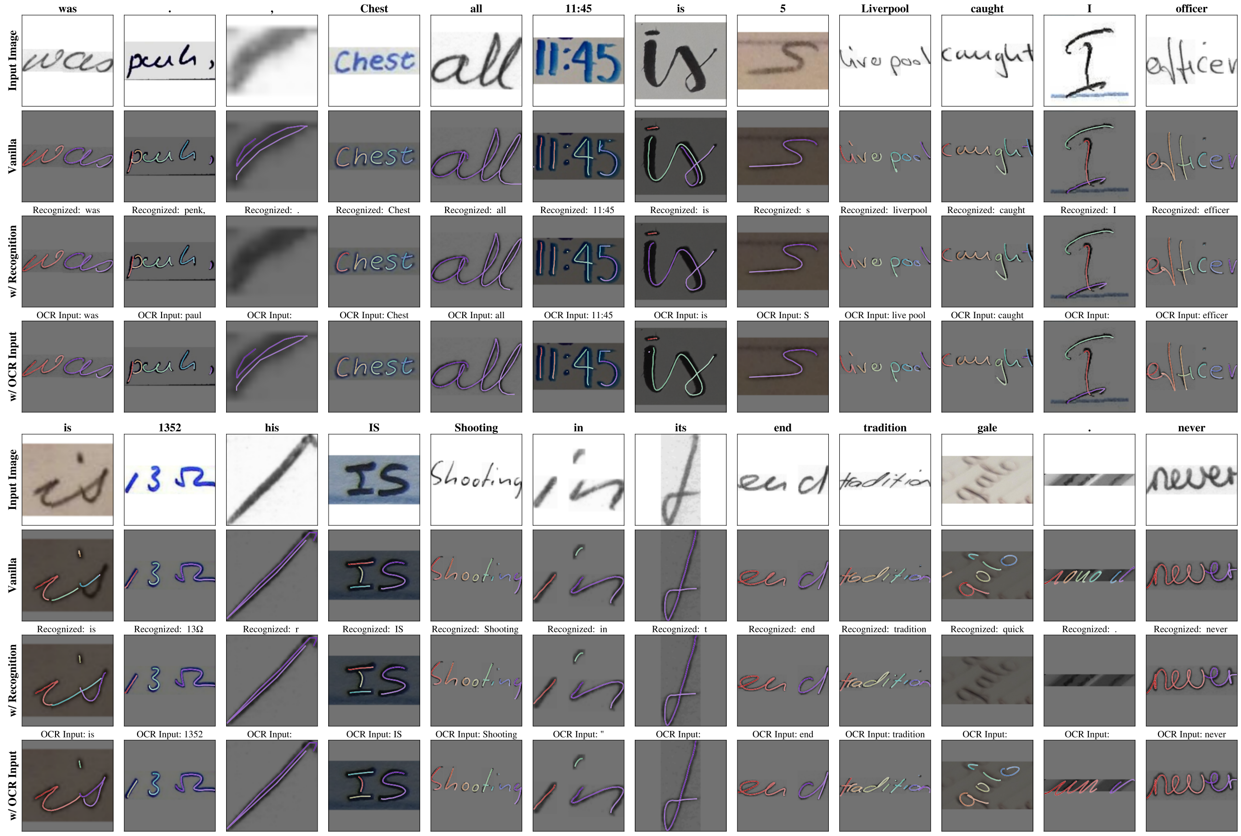

Figure 45: Results of **Small-p** on randomly selected samples from 3 public evaluation datasets.

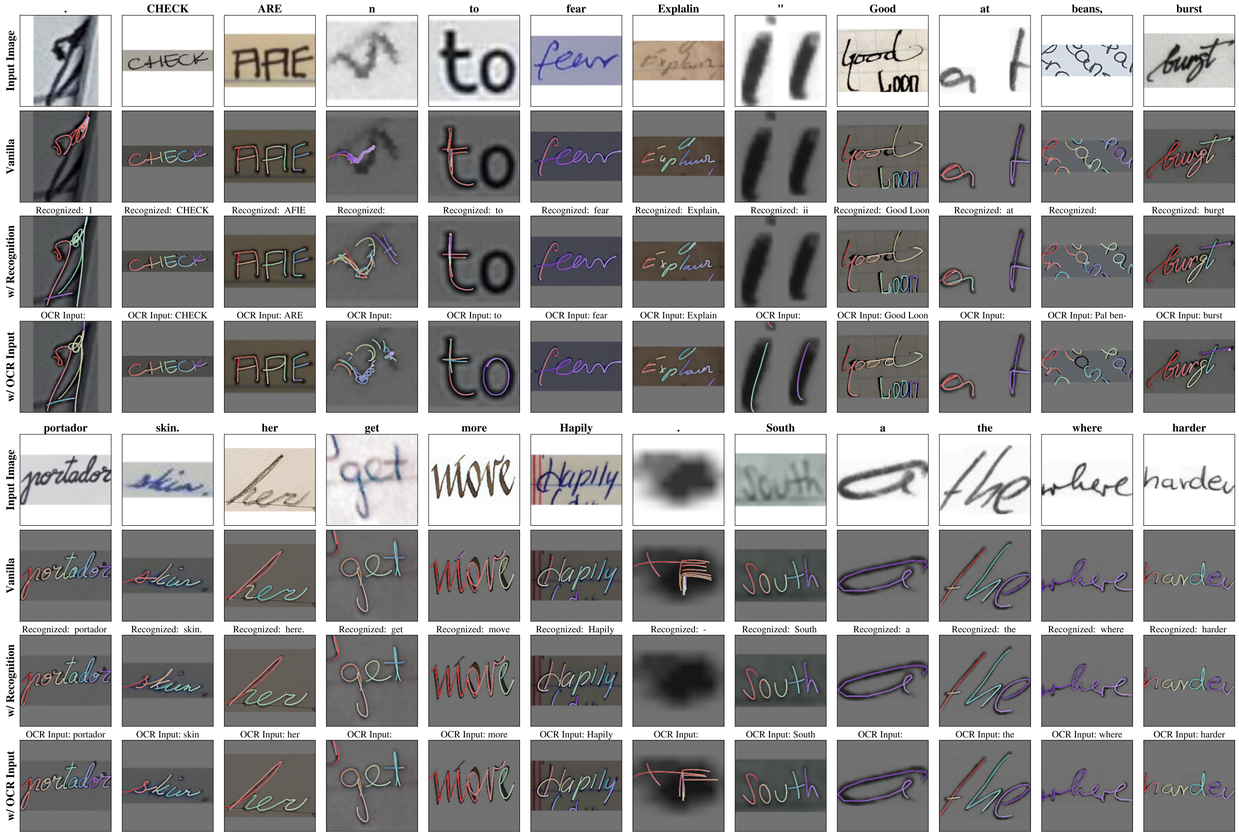

Figure 46: Results of **Small-i** on randomly selected samples from 3 public evaluation datasets.

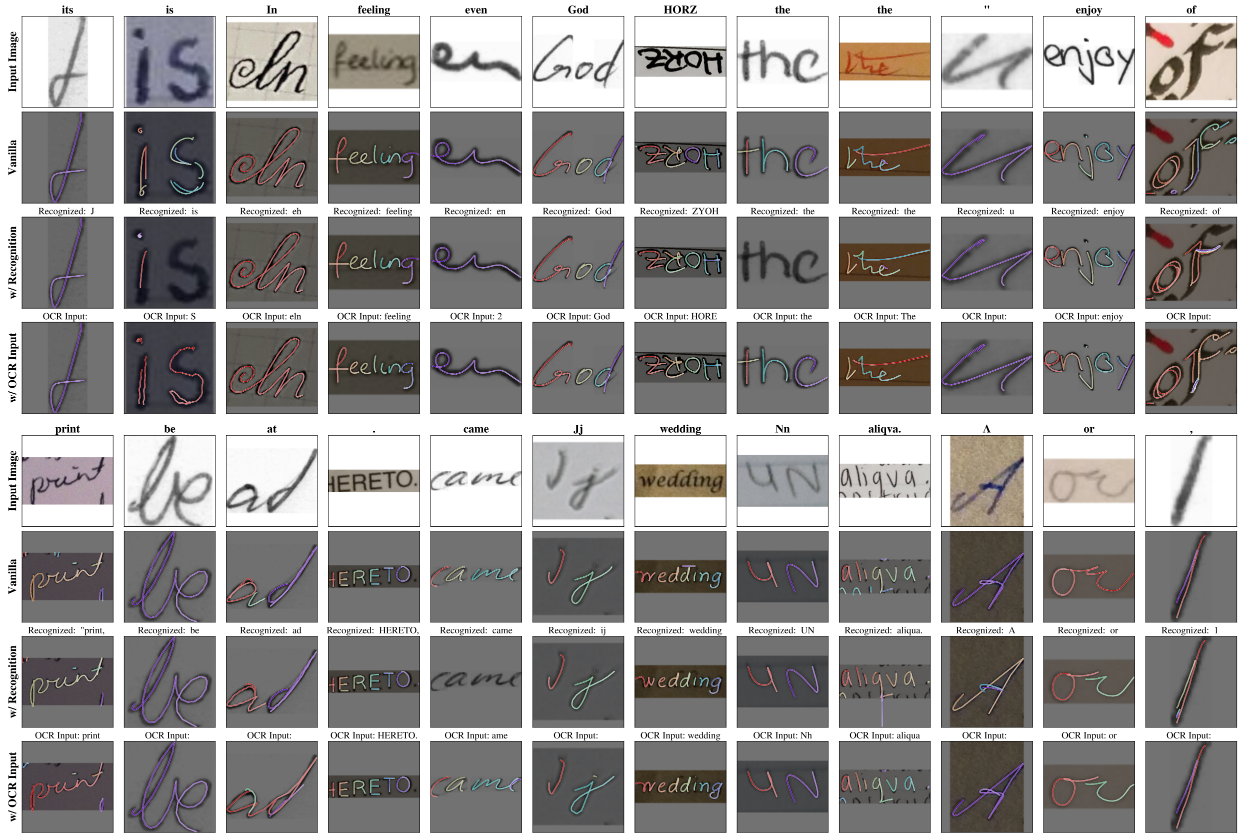

Figure 47: Results of **Large-i** on randomly selected samples from 3 public evaluation datasets.

M.1 More Visualizations on Public Evaluation Datasets

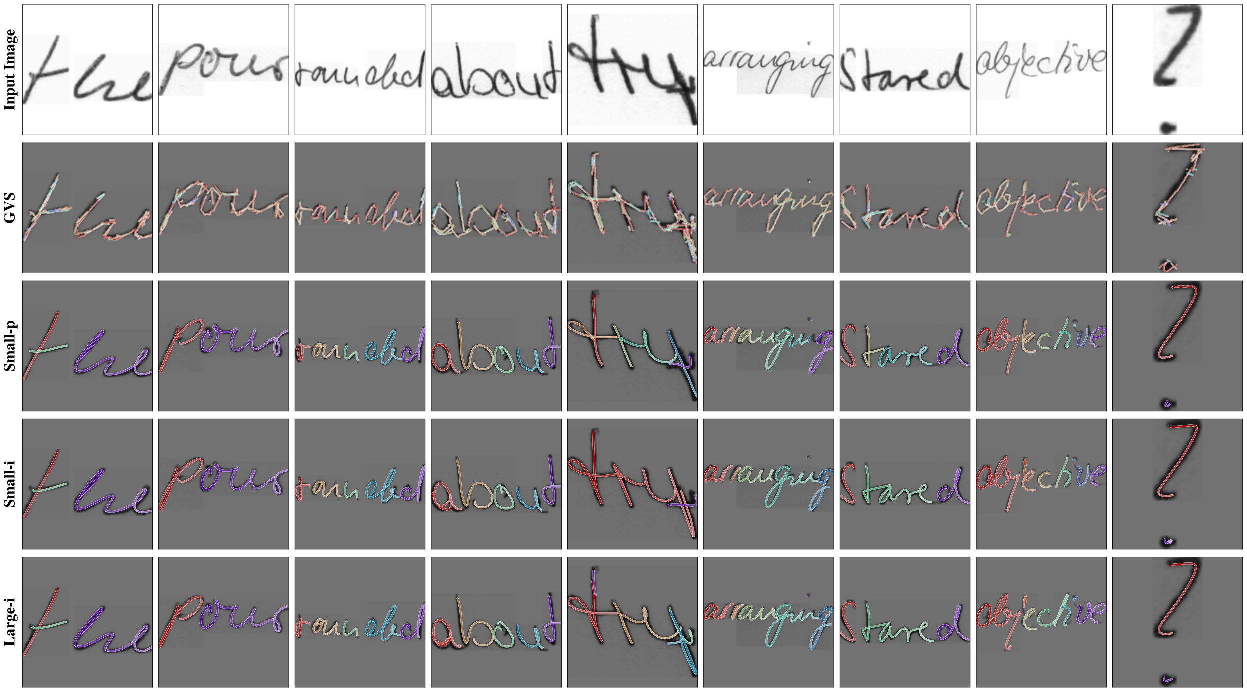

Figure 48: Comparison between **Small-i**, **Small-p**, and **Large-i** on IAM Dataset.

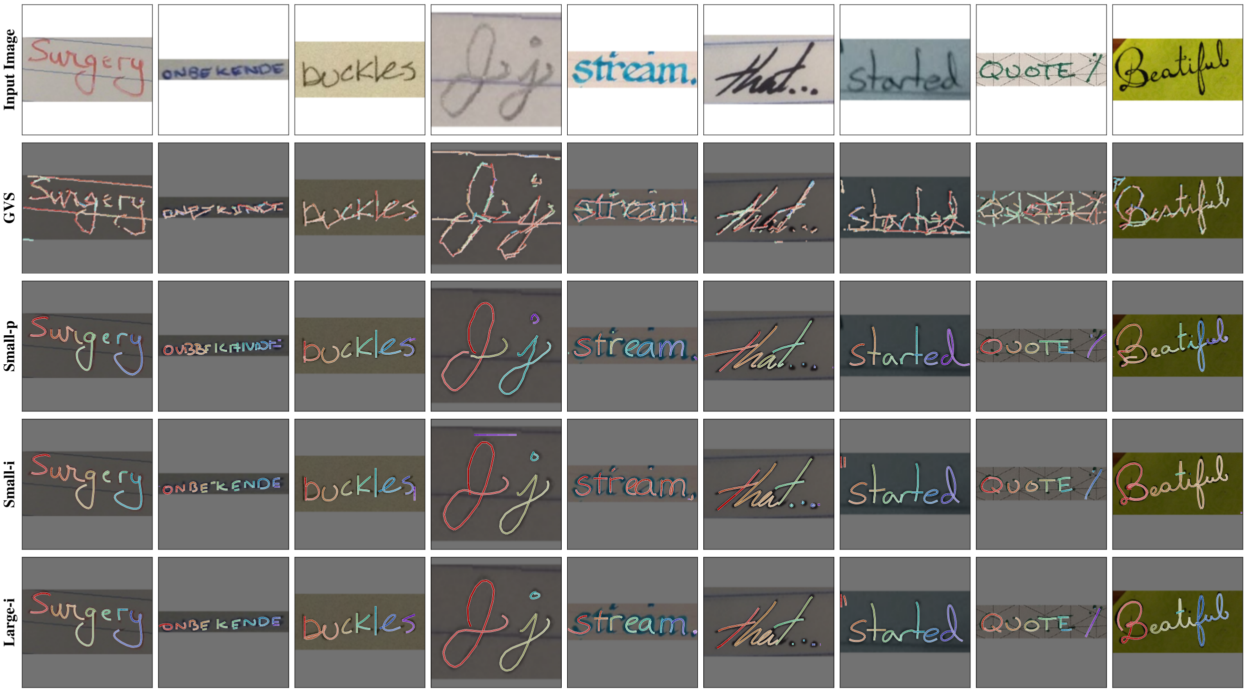

Figure 49: Comparison between **Small-i**, **Small-p**, and **Large-i** on IMGUR5K Dataset.

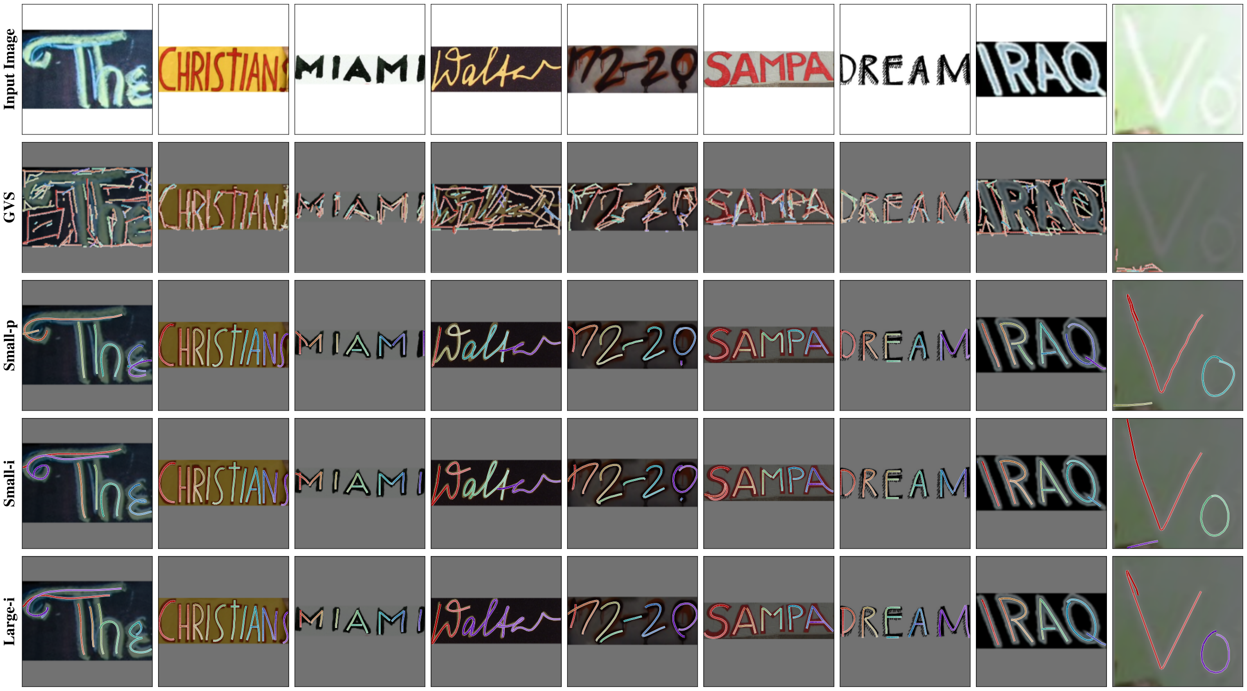

Figure 50: Comparison between **Small-i**, **Small-p**, and **Large-i** on HierText Dataset.

N Impact Statements

N.1 Ethical Considerations

Proposed model can not be used for open-ended generation. We verify that proposed models are unable to perform open-ended ink generation. We provide random texts in task prompts of task *Derender with Text* (in Figure 3) with input images either empty or contain handwritings that do not match the label. We observe that the generated inks do not match the labels for 100 cases inspected, signifying that the model is unable to generate the prompted text that is not present in the input image. More details in Appendix N.3.

N.2 Future Societal Consequences

Our work could allow access to the digital ink underlying the physical notes, potentially enabling the training of better online handwriting recognizers for languages that are historically low-resource in the digital ink domain.

N.3 Open-ended Generation

As illustrated in Figure 51, our experiments with **Small-p**, **Small-i**, and **Large-i** models demonstrate that when prompted with text not present in the original image, the models fail to generate accurate corresponding handwritten strokes. This behavior acts as a natural safeguard against potential misuse, such as forgery or unauthorized reproduction of handwriting styles. Since the models can only reconstruct handwriting patterns from the input image rather than generating arbitrary new content, they inherently restrict attempts to synthesize fraudulent handwritten content.

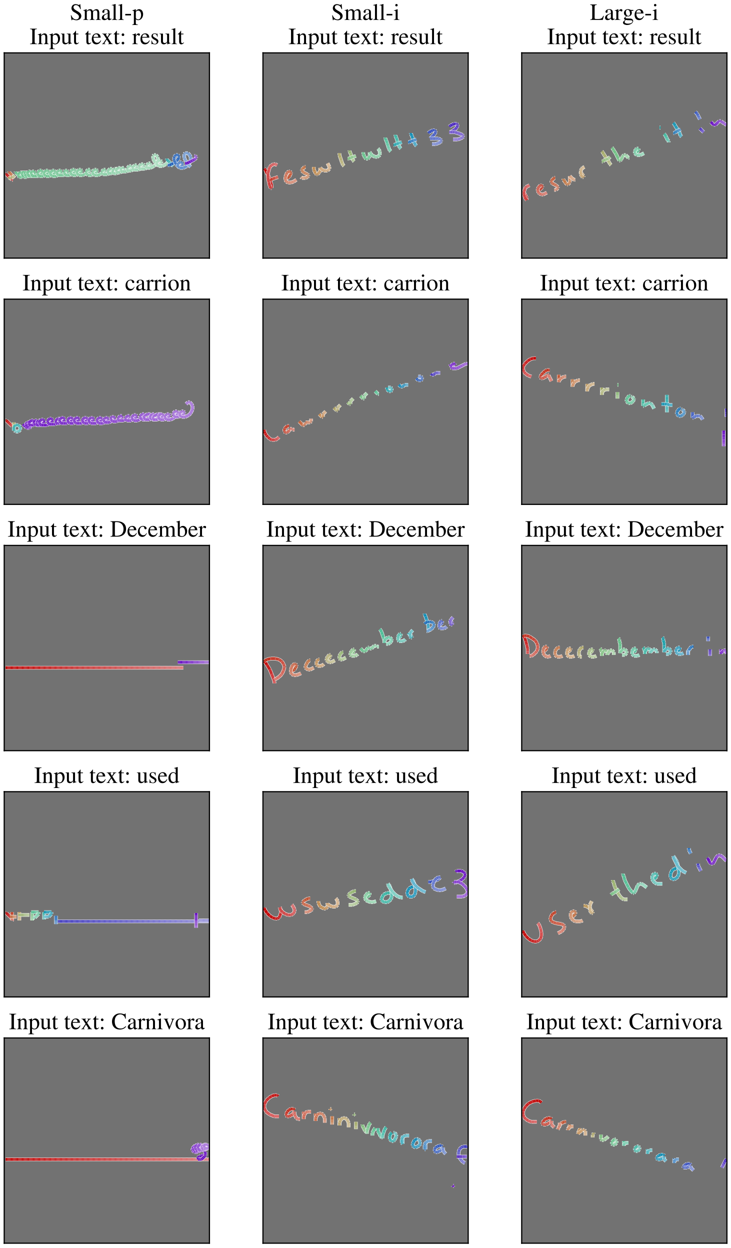

Figure 51: **Inability to perform open-ended generation.** Prompting **Small-p**, **Small-i** and **Large-i** with text that is not presented in the image does not produce digital inks that match the textual input.